國 立 交 通 大 學

電 子 物 理 研 究 所

碩 士 論 文

二維 cubic-k Dresselhaus-type 電子系統中在圓盤附近的量子散射

QUANTUM SCATTERING FROM A CIRCULAR DISK IN A CUBIC-K DRESSELHAUS-TYPE TWO DIMENSIONAL ELECTRON GAS

研 究 生：杜冠誼

指導教授：朱仲夏教授

中華民國九十八年七月

二維 cubic-k Dresselhaus-type 電子系統中在圓盤附近的量子散射

QUANTUM SCATTERING FROM A CIRCULAR DISK IN A CUBIC-K DRESSELHAUS-TYPE TWO DIMENSIONAL ELECTRON GAS

研 究 生：杜冠誼　　Student：Kuan-Yi Tu

指導教授：朱仲夏教授　　Advisor：Prof. Chon Saar Chu

國 立 交 通 大 學

電 子 物 理 研 究 所

碩 士 論 文

A Thesis
Submitted to Department of Electrophysics
College of Science
National Chiao Tung University
in Partial Fulfillment of the Requirements
for the Degree of
Master
in
Electrophysics

July 2009
Hsinchu, Taiwan, Republic of China

中華民國九十八年七月

二維 cubic-k Dresselhaus-type 電子系統中在圓盤附近的量子散射

研究生：杜冠誼　　指導教授：朱仲夏教授

國立交通大學

電子物理研究所

摘要

此論文的工作一直致力解讀在一個圓盤微結構附近，考慮 Dresselhaus 型自旋軌道耦合作用下自旋相關的散射效應。Dresselhaus 型自旋軌道耦合作用在這裡主要包括了 linear-k 相關以及 cubic-k 相關的貢獻。

以分波方法為基礎，在散射區間內經計算後可以得到完整散射後的波函數。透過調查入射電子平面波後，DSOI 造成空間辨別的散射效應，linear-k 與 cubic-k DSOI 貢獻的差異可以明顯地被辨識，同時得到所對應的能量耗散關係。在我們的發現：對於 linear-k Dresselhaus，電子自旋密度與機率密度分佈擁有空間對稱性輪廓，與平面波入射角度無關。相反地，在 cubic-k Dresselhaus SOI 例子中明顯地表示出與平面波入射角度相關。

特別地，若入射平面波角度為幾個特定的角度，我們可以發現有相似的電子自旋密度對應在 cubic-k Dresselhaus 例子與 linear-k Dresselhaus 例子之間。

QUANTUM SCATTERING FROM A CIRCULAR DISK IN A CUBC-K DRESSELHAUS-TYPE TWO DIMENSIONAL ELECTRON GAS

Student: Kuan-Yi Tu Advisor: Prof. Chon-Saar Chu

Department of Electrophysics

National Chiao Tung University

Abstract

This thesis work has devoted to the study of spin-dependent scattering effects from a circular-disk microscopic structure with Dresselhaus-type spin-orbit coupling. The Dresselhaus spin-orbit coupling considered here includes both contributions terms for one is linear-k dependence and the other is cubic-k dependence.

Based on the method of partial waves, the complete scattering wave function in a circular scattering region can be rigorously derived and obtained. Through investigating their spatial-resolved scattering behaviors from linear and cubic Dresselhaus-type SOI disk under the electron plane wave incidence, different DSOI contributions can be apparently discerned, and their corresponding detail energy dispersion relationships as well. In our findings: for linear-k Dresselhaus case, the spin density and probability density distributions own their spatial symmetry profile, which is featured independence of the plane wave incident angle. On the contrary, strong incident angle dependence is manifested for the case of cubic-k Dresselhaus spin-orbit interaction.

In particular , for incidence plane wave in some characteristic angle, we can find similar spin density responses between cubic-k Dresselhaus case and linear-k Dresselhaus case.

致謝

感謝朱老師兩年來教導，謹慎細密的研究態度與研究的熱忱，讓我獲益良多。也感謝老王學長在研究中給我的協助與討論，唐志雄學長在關鍵的時期給予我最寶貴的意見以及想法。多虧有實驗室夥伴興哥、fat、布達、小明、偉哥帶給我的歡樂，才能在研究外有多餘的樂趣，也感謝實驗室夥伴對於我一些無理或固執行為的包含。最後特別，感謝興哥在這兩年中對我人生的想法態度上的開導，讓我無論對人對事多有一番體悟。謝謝我的家人，謝謝我的朋友，感謝所有幫助我關心我的人。

Contents

Abstract in Chinese **i**

Abstract in English **ii**

Acknowledgement **iii**

1 Introduction **1**

1.1 Background : types of spin-orbit coupling system in solid state system . . 2

1.2 Motivation : cubic-k Dresselhaus spin-orbit interaction (SOI) 3

1.3 A simple guide to thesis 3

2 Two dimensional Dresselhaus-type SOI electron system **5**

2.1 Linear-k Dresselhaus SOI 6

2.1.1 Incident plane wave 7

2.1.2 Cylindrical form representation of the eigenstates 12

2.2 Cubic-k Dresselhaus SOI 14

2.2.1 Incident plane wave 14

2.2.2 Cylindrical form representation of the eigenstates 17

2.3 Energy dispersion of Dresselhaus SOI system 20

2.4 BIA in spin splitting in 2D systems 24

2.5 Connection between linear-k DSOI and ROSI systems 25

3 Scattering from a cylindrically symmetric potential in a Dresselhaus SOI

system **28**

3.1 Cubic-k Dresselhaus SOI 29

3.1.1 Coupled cylindrical wave representations of the incoming wave . . . 29

3.1.2 Coupled cylindrical wave representations of the outgoing wave . . . 31

3.2 Linear-k Dresselhaus SOI 36

3.2.1 Coupled cylindrical wave representations 36

3.3 Scattering of the scattering state 39

3.4 Spin density of the scattering state 39

3.5 Particle continuity equation 41

4 Numerical results and discussions **44**

4.1 Results for linear-k Dresselhaus SOI 44

4.2 Results for cubic-k Dresselhaus SOI and more Discussions 48

4.3 Discussion on the connection of spin density with the plane wave direction 49

5 Future work **50**

A Simplify the boundary condition problem **51**

B Derivation of spin density of the total wave function after scattering **55**

C Comparison of analytical results and numerical approach for cylindrical wave case **60**

List of Figures

2.1 Radial profile of "hard" wall disk of our system. 8

2.2 Energy dispersion with helicity η for a linear-k Dresselhaus system ; the blue line correspond to $\eta = +$ and the red line correspond to $\eta = -$. The dash line means that system has no spin-orbit coupling ($\beta_1 = 0$) and Eq. (2.5) represents two parabolic bands centered up $k = -\eta\frac{(\beta_1\kappa^2)}{2}$. 9

2.3 The plane wave of an incident electron wave with wave vector $\mathbf{k}$ making an angle φ_k with $\hat{x}$ axis gets scattered by a scattering region defined by a Dresselhaus SOI and a "hard" wall disk. 10

2.4 Dispersion relation for a 2D Dresselhaus-type system (includes linear and cubic terms) and the Dresselhaus constant $\beta = 27\text{eV}\,\mathring{\text{A}}^3$ and $d = 15nm$. . . 21

2.5 Dispersion relation for a 2D Dresselhaus-type system (includes linear and cubic terms) and the Dresselhaus constant $\beta = 27\text{eV}\,\mathring{\text{A}}^3$ and $d = 15nm$ in the larger k range. 22

2.6 The roots of the energy dispersion Eq. (2.35) where $\varphi_k = \frac{\pi}{3}$ and $\eta = +$. The right pattern is the real part of k and the left pattern is the imagine part of k. In the central region of the real k and k imagine pattern show that the three roots in the region are all pure real values. Apparently, the momentum k we have to neglect is only the smallest one due to the corresponding much fast oscillation and then the others are exactly we must consider. 24

2.7 the $[x', y']$ system is rotated by angle θ, retaliative to the $[x, y]$ system. . . 26

4.1 Distribution of the out-of-plane spin density S_z. The plane wave incident a hard wall disk in linear-k Dresselhaus system with the helicity $\eta = +$, the incident energy ε=7.7, and the incident angle φ_k=0. Lighter regions means the region whose spin density S_z >0 (spin up). And the darker regions represent the region of spin down 45

4.2 The spatial dependence of the magnitude of the total wave function probability density. Out of the white circle is the region with finite Dresselhaus SOI. Apparently, when the plane wave propagates along the x axis, the probability density is almost zero behind the disk due to the hard wall disk . 46

4.3 Distribution of the out-of-plane spin density S_z. The plane wave incident a hard wall disk in linear-k Dresselhaus system with the helicity $\eta = +$, the incident energy ε=13.23, and the incident angle φ_k=0. Lighter regions means the region whose spin density S_z >0 (spin up) . And the darker regions represent the region of spin down 47

4.4 The spatial dependence of the magnitude of the total wave function probability density. Out of the white circle is the region with finite Dresselhaus SOI. Apparently, when the plane wave propagates along the x axis, the probability density is almost zero behind the disk due to the hard wall disk. 47

4.5 The quality the spin density S_z determining the number m as function of φ for a central hard wall disk where m represents the number of the partial waves we must sum. Apparently, the line of the spin density corresponding to the distribution of the spin density Fig. 4.1 at r=2 is saturated for a larger m. And the probability density also has the same situation. 48

C.1 Comparison of analytical results and numerical approach for cylindrical wave case of m_{in}=1: (a) $N = 11$, (b) $N = 45$, (c) $N = 47$ and (d) $N = 49$. 64

C.2 Comparison of analytical results and numerical approach for cylindrical wave case of m_{in}=3 : (a) $N = 49$ and (b) $N = 51$. 65

C.3 Comparison of analytical results and numerical approach for cylindrical wave case of m_{in}=7: (a) $N = 129$ and (b) $N = 131$. 65

C.4 Comparison of analytical results and numerical approach for cylindrical wave case of m_{in}=11 : (a) $N = 133$ and (b) $N = 135$. 65

C.5 Comparison of analytical results and numerical approach for cylindrical wave case of m_{in}=1 : (a) $N = 63$ and (b) $N = 65$. 66

Chapter 1

Introduction

The spin dependence of the electronic properties of mesoscopic technology and artificial nano-structure is one of leading problem nowadays in the physics of electric devices. In this way, taking account of spin property of electrons are the improvement of actual devices. To develop spintronic device in spintronics, quantum information, and other applications is necessary to understand how the transport of electron affect its spin and further control conditions on the manipulation of the spin orbit interaction in the semiconductor macrostructure. The interaction causes the decay of spin polarization since the spin-orbit coupling breaks the total spin symmetry [1]. Accordingly, we must understand the spin-orbit coupling [2].

In semiconductor with strong SOI, the energy eigenstates are spin dependent and can have apparently spin splitting without a magnetic field for electrons when there exits inversion asymmetry. And then the effect in the low dimensional structure becomes larger where the inversion asymmetry controlled. It is known that in a variety of systems we consider that changing the spin properties of an incident beam of particle in scattering experiment. The spin-orbit interaction cause asymmetry of the differential scattering cross section (skew scattering). In addition, the SOI also changes the polarization vector of the incident beam.

1.1 Background : types of spin-orbit coupling system in solid state system

There are two types of spin-orbit interaction in semiconductor according to the physical origan. One is intrinsic type such as Rashba spin orbit interaction (RSOI) [3] induced by structure inversion asymmetry (SIA) and the other is extrinsic type such as Drsselhaus spin orbit interaction (DSOI) [4] induced by bulk inversion asymmetry (BIA) of the crystal lattice. The effect produced by the interplay between Dresselhaus and Rashba spin-orbit interactions on spin relaxation has been studied in a few publications [5–7]. Furthermore , there are a few works on the transport properties of two-dimensional electron gas [8–11] . Especially, Datta and Das proposed a spin-field-effect transistor (SFET) [12] for quasi-1D ballistic wires with Rashba coupling . In thin quantum wells, the strength of the DSOI is compatible to the strength of the RSOI. The special spin symmetry arises due to the translational invariance in the longitudinal coordinate in quantum wires is used to propose a transport experiment to measure the strengths of the Rashba and the Dresselhaus interaction for any chosen polarization [13]. There are a few works on the effects of the competition between two types of SOI on the transport properties in mesoscopic rings [14, 15].

A promising spin transistor application has been proposed that the strength of the RSOI can be tuned by external gates voltages or asymmetric doping and this initiated intensive research in spintronics [16]. Schliemann, Egues, and Loss proposed a SFET [17] that can operate in diffusive quasi-2D systems based on tuning Rashba and linear Dresselhaus terms to be equal in strength, which produces long spin lifetime , neglecting cubic Dresselhaus term. On the other hand, recent studies have been devoted to the physical consequences of the interplay of the RSOI and impurity [18]. Recently, the intrinsic spin Hall effect (SHE) [19, 20] as been established in a spin-orbit coupled p-doped semiconductor and in a Rashba spin-orbit coupled two-dimensional electron systems was predicted theoretically.

1.2 Motivation : cubic-k Dresselhaus spin-orbit interaction (SOI)

In quasi-2D systems, Dresselhaus terms has two components, one linear in the momentum and the other cubic. The cubic Dresselhaus contribution [21] is often neglected since it is smaller apparently than the linear Dresselhaus contribution. Nevertheless , the strength of the SO terms are difficult to measure so that to obtain a full understanding of their strength is crucial . In addition, in confined system such as quantum dot, quantum wire, some effect of the linear Dresselhaus SOI are suppressed, so it is important to know the contribution from the cubic Dresselhaus SOI which is helpful to develop spintronic devices.

Theoretically, the spin current is the important physical quantity in spintronics, and it has been extensively studied [22–24] . Many fundamental phenomena, such as the SHE and the spin precession in systems with spin-orbit coupling have been discovered . There are many recent works on spin dependent quantum scattering [25] around microstructures [26–28]. In this thesis , we study the scattering of the scattering of electrons by a disk in 2DEG with Dresselhaus spin-orbit coupling.

1.3 A simple guide to thesis

In Chapter 2 , we will solve the eigenstate problem in two dimensional Dresselhaus-type system including linear-k and cubic-k DSOIs, so that the energy dispersion can be obtained. In addition , the eigenstates would be represented in cylindrical form due to the cylindrical symmetry potential .We consider that the plane wave which is the eigenstate of Dresselhaus-type Hamiltonian incident a hard wall disk in DSOI system. At such, we can make a connection between linear-k Dresselhaus and Rashba Hamiltonian.

In Chapter 3, we introduce the method of partial waves for a scattering. The total waves are composed of incoming waves and outgoing waves, where the incoming wave part is given by the incident plane wave and then outgoing wave part can be represented

by the eigenstate which we obtained in Chapter 2. Furthermore, the outgoing wave part contains unknown coefficients which are contributed from the two kinds of helicity wave functions. The unknown coefficients can be obtained by solving the boundary condition problems. Finally, we obtain the particle current density by driving the particle continuity equation of the Dresselhaus-type system .

In Chapter 4, the numerical results show the spin density or other quantities after scattering by a hard wall disk both in linear-k and cubic-k DSOI. Therefore, we can use the result to evaluate the cubic-k contribution during the scattering process by comparing the results only for linear-k Dresselhaus and the results includes cubic-k Dresselhaus. Also, we discuss the connection between spin density and the plane wave direction.

In Chapter 5, we present possible work about spin-orbit interaction in Dresselhaus or Rashba system.

Chapter 2

Two dimensional Dresselhaus-type SOI electron system

In this chapter we present a theoretical study of electron scattering in two dimensional Dresselhaus-type SOI electron system. Using the spin dependent method of partial waves [29] the complete scattering wave function is derived exactly for the case of a circular region. For a 2D central potential (hard wall disk), the cylindrical symmetry governs that the wavefunction is expressed most conveniently in polar coordinates. There exit linear-k DOSI and cubic-k DOSI in Dresselhaus-type SOI and mostly cubic-k DOSI is neglected. At the same time, linear-k DSOI can be compare with that Rashba-type spin orbit interaction (ROSI) that we can make a connection between them. The competition of two types of SOI on the transport properties of two dimensional electron gas are interesting and highly desirable.

In our numerical examples, physical parameters are chosen according to practical experimental situation and for the material GaAs. Parameters units typical for GaAs are: electron density n =2.51 $\times 10^{11}\,\mathrm{cm}^{-2}$; energy units $\varepsilon^* = 8.977\,\mathrm{meV}$; m* =0.067 m_e; Dresselhaus strength β^*= 4553 eVA^3; k^*= 1.25 $\times 10^8\, m^{-1}$; disk radius $R = 50\ nm$; wide scale d=25nm.

Units

In order to simplify our calculation, in the following expression that all the physical quantities are dimensionless in units according to a typical carrier concentration $n = 6.98\times 10^{15}\mathrm{m}^{*-2}$. The wave vector is in unit of Fermi wavelength $k^* = \sqrt{2\pi n}$; length in the unit of $1/k^*$; energy E in the unit of Fermi energy $\varepsilon^* = \frac{\hbar^2 k_F^2}{2m^*}$; Dresselhaus constant in the unit of $\beta^* = \frac{\hbar^2}{2m^* k_F}$. The Hamiltonian for a 2D potential in the Dresselhaus SOI type system has the form

$$H = \frac{-\hbar^2}{2m^*}\nabla^2 + \beta k_x(k_y^2 - \kappa^2) - \beta k_y(k_x^2 - \kappa^2) + V(x, y) \tag{2.1}$$

where m^* is the effective electron mass, $V(x, y)$ is the 2D potential, β is Dresselhaus spin orbit constant, and $\kappa = \frac{\pi}{d}$.

Affer a standard dimensionless process, we can obtain a dimensionless Hamiltonian

$$\hat{H} = -\nabla^2 + \beta k_x(k_y^2 - \kappa^2) - \beta k_y(k_x^2 - \kappa^2) + V(x, y) \quad . \tag{2.2}$$

Frist, we investigate the incident plane wave in 2D Dresselhaus-type SOI electron system including linear k and cubic k and then make a connection between Dresselhaus SOI and Rashba SOI.

2.1 Linear-k Dresselhaus SOI

According to the physical origin of the SOI, the SOI can be divided into intrinsic and extrinsic types. The intrinsic type is Rashba which arises from SIA or Dresselhaus interaction which arises from BIA. The extrinsic SOI is due to the presence of SOI scatterers in the system. In quasi-two-dimensional systems, the Dresselhaus SOI includes two components, the linear part and the cubic part in momentum. The cubic Dresselhaus term is usually neglected, as it is much smaller than the linear term contribution. We present a similar model to deal with a Dresselhaus spin-oribit coupling system in which we consider

Dresselhaus linear k.

2.1.1 Incident plane wave

The Hamiltonian for a 2DEG in the presence of the Dresselhaus spin-orbit interaction with a circular disk at the origin is given by

$$\hat{H} = -\nabla^2 - \kappa^2\beta_1(\hat{k}_x\sigma_x - \hat{k}_y\sigma_y) + V(x,y) \quad , \tag{2.3}$$

where σ_j are the Pauli matrices and β_1 is the Dresselhaus spin-orbit coupling constant . The eigenstates and corresponding eigenvalues for a free-particle Hamiltonian (outside the disk) with Dresselhaus spin-orbit coupling, are given by

$$\psi_{in,\eta}(\phi_k) = e^{i\mathbf{k}\cdot\mathbf{r}}\chi_\eta \tag{2.4}$$

$$\varepsilon = k^2 + \eta(\beta_1\kappa^2)k \quad , \tag{2.5}$$

where

$$\tan(\varphi_k) = \frac{k_y}{k_x} \quad , \tag{2.6}$$

$$\chi_\eta = \frac{1}{\sqrt{2}}\begin{pmatrix} 1 \\ \eta\Re \end{pmatrix} \quad helicity\, \eta = \pm \quad , \tag{2.7}$$

and

$$\Re = -e^{-i(\varphi_k)} \quad . \tag{2.8}$$

And the only assumption for the scattering potential (see Fig. 2.1) is that

$$V(x,y) = V(\mathbf{r}) = \begin{cases} 0 \ , \ r > R \\ \infty \ , \ r \leq R \end{cases} \quad . \tag{2.9}$$

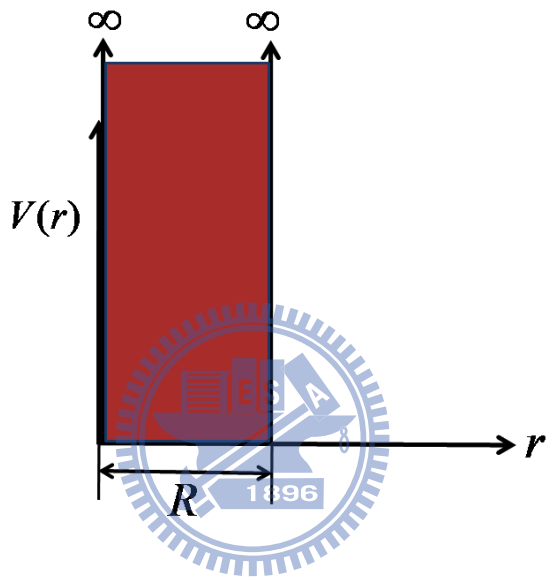

Figure 2.1: Radial profile of "hard" wall disk of our system.

The dispersion relation in Eq. (2.5) represents two parabolic bands Fig. 2.2 centered up $k = -\eta\frac{(\beta_1\kappa^2)}{2}$. For states propagating with their momentum $\mathbf{k}$ making a angle φ_k with respect to the $\hat{x}$ axis Fig. 2.3 and for an energy $E \geq 0$, there exit a degenerate states which is

$$\psi_{in,+} = \frac{1}{\sqrt{2}} \begin{pmatrix} 1 \\ \Re \end{pmatrix} e^{i\mathbf{k}\cdot\mathbf{r}} \quad , \tag{2.10}$$

$$\psi_{in,-} = \frac{1}{\sqrt{2}} \begin{pmatrix} 1 \\ -\Re \end{pmatrix} e^{i\mathbf{k}'\cdot\mathbf{r}} \quad , \tag{2.11}$$

where $\overrightarrow{k} = k\,[\cos(\varphi_k)\hat{x} + \sin(\varphi_k)\hat{y}]$ and $\overrightarrow{k'} = k'\,[\cos(\varphi_k)\hat{x} + \sin(\varphi_k)\hat{y}]$ whom we can get by solving $\varepsilon = k^2 + \beta_1 k\kappa^2 = k'^2 - \beta_1 k'\kappa^2$.

The states $\psi_{in,+}$ represent plane wave states with helicity ($\eta = +$) whose spin states are perpendicular to the momentum direction. The detail derivation of the eigenstates and eigenvalues is in the appendix.

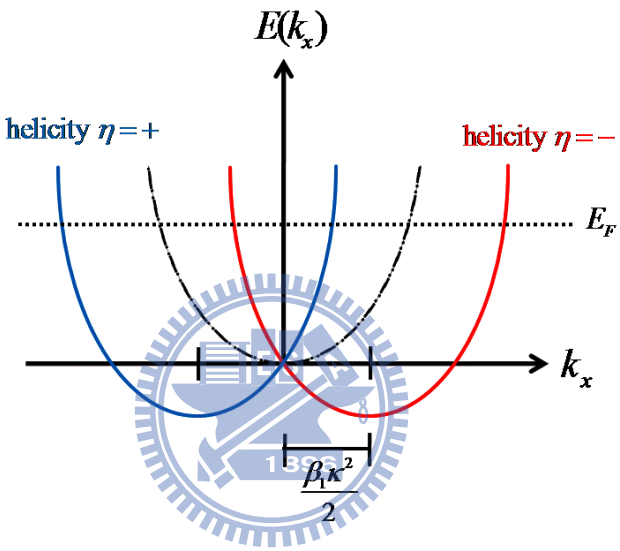

Figure 2.2: Energy dispersion with helicity η for a linear-k Dresselhaus system ; the blue line correspond to $\eta = +$ and the red line correspond to $\eta = -$. The dash line means that system has no spin-orbit coupling ($\beta_1 = 0$) and Eq. (2.5) represents two parabolic bands centered up $k = -\eta\frac{(\beta_1\kappa^2)}{2}$.

A plane wave corresponding to an free electron propagating with the momentum vector $\overrightarrow{k}$ making a propagating angle φ_k with $\hat{x}$ axis, in accordance with Jacobi-Anger expansion [30] which can be expanded as a linear superposition of the circular free waves

$$e^{i\mathbf{k}\cdot\mathbf{r}} = e^{ikr\cos(\varphi-\varphi_k)} = \sum_{m=-\infty}^{\infty} i^m J_m(kr) e^{im(\varphi-\varphi_k)} \ . \tag{2.12}$$

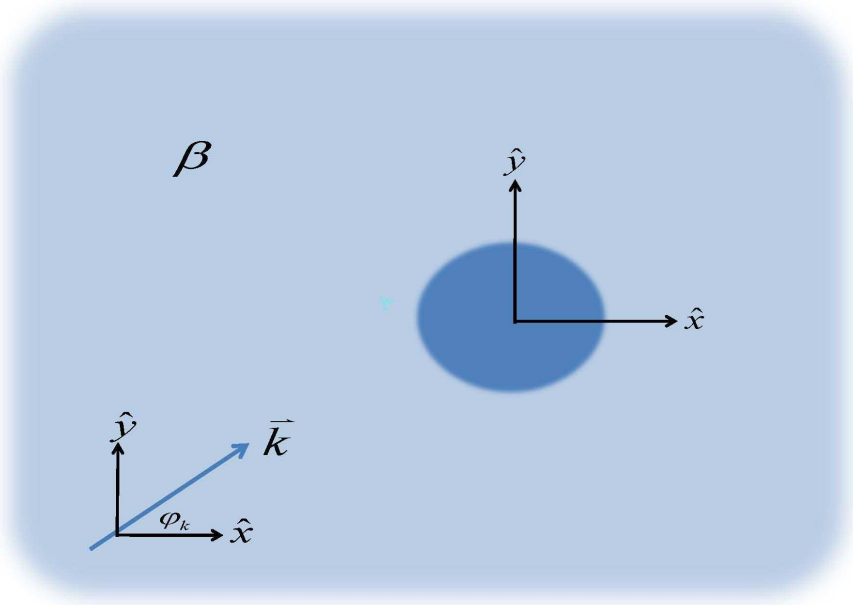

Figure 2.3: The plane wave of an incident electron wave with wave vector **k** making an angle φ_k with $\hat{x}$ axis gets scattered by a scattering region defined by a Dresselhaus SOI and a "hard" wall disk.

Then the incident plane wave with momentum k and helicity $(\eta = +)$ can be decomposed as the following linear superposition:

$$\psi_{in,+} = \frac{1}{\sqrt{2}} \sum_{m=-\infty}^{\infty} \begin{pmatrix} i^m J_m(kr) e^{im(\varphi-\varphi_k)} \\ (+\Re) i^{m-1} J_{m-1}(kr) e^{i(m-1)(\varphi-\varphi_k)} \end{pmatrix} \tag{2.13}$$

Since Bessel function $J_m(kr)$ is a standing wave along the radial direction, for our purpose, it is easily to express it in terms of two radial propagating waves, the Hankel functions,

$$J_m(kr) = \frac{1}{2}\left[H_m^{(1)}(kr) + H_m^{(2)}(kr)\right] \ , \tag{2.14}$$

where the first kind and the second Hankel functions are defined as

$$\begin{aligned} H_m^{(1)}(z) &= J_m(z) + iY_m(z) \ ; \\ H_m^{(2)}(z) &= J_m(z) - iY_m(z) \ . \end{aligned} \tag{2.15}$$

In the region where $kr \gg 1$ the radial propagating dependence of these Hankel functions become most apparent in their asymptotic form,

$$\begin{aligned} \lim_{kr\to\infty} H_m^{(1)}(kr) &\sim \tfrac{1}{\sqrt{kr}} e^{ikr} \quad ; \\ \lim_{kr\to\infty} H_m^{(2)}(kr) &\sim \tfrac{1}{\sqrt{kr}} e^{-ikr} \ . \end{aligned} \tag{2.16}$$

For large r, $H_m^{(1)}(kr)$ goes like e^{ikr}/r, we can regard it as a circular waves propagating radial outwards from the scattering center. In the same way, $H_m^{(2)}(kr)$ can be treated as a circular waves propagating radial inwards from the scattering center.

To consider the scattering process for the cylindrical symmetric potential, we decompose Bessel function $J_m(kr)$ (**standing waves**) as Hankel functions $H_m^{(2)}(kr)$ (**incoming waves**) and $H_m^{(1)}(kr)$ (**outgoing waves**) so Eq. (2.13) become

$$\psi_{in,+} = \frac{1}{2\sqrt{2}} \sum_{m=-\infty}^{\infty} \begin{pmatrix} i^m \left[H_m^{(2)}(kr) + H_m^{(1)}(kr) \right] e^{im(\varphi-\varphi_k)} \\ (+\Re) i^{m-1} \left[H_{m-1}^{(2)}(kr) + H_{m-1}^{(1)}(kr) \right] e^{i(m-1)(\varphi-\varphi_k)} \end{pmatrix} \tag{2.17}$$

or

$$= \frac{1}{2\sqrt{2}} \sum_{m=-\infty}^{\infty} i^m \begin{pmatrix} \left[H_m^{(2)}(kr) + H_m^{(1)}(kr) \right] e^{im(\varphi-\varphi_k)} \\ (-i\Re) \left[H_{m-1}^{(2)}(kr) + H_{m-1}^{(1)}(kr) \right] e^{i(m-1)(\varphi-\varphi_k)} \end{pmatrix} \tag{2.18}$$

where

$$\Re = -e^{-i\varphi_k} \quad .$$

For the general case, the incident wave propagates along $\hat{x}$ axis ($\varphi_k = 0$) with positive

helicity, the wave function is given by

$$\psi_{in,+} = \frac{1}{2\sqrt{2}} \sum_{m=-\infty}^{\infty} i^m \begin{pmatrix} \left[H_m^{(2)}(kr) + H_m^{(1)}(kr)\right] e^{im(\varphi)} \\ (i)\left[H_{m-1}^{(2)}(kr) + H_{m-1}^{(1)}(kr)\right] e^{i(m-1)(\varphi)} \end{pmatrix} \tag{2.19}$$

The cylindrical symmetry of the scattering potential cause waves to be coupled only with the same m . This essentially the conservation of the conservation of orbital angular momentum, which is true for a center potential but no SOI.

2.1.2 Cylindrical form representation of the eigenstates

In cylindrical coordinates, which are useful when we consider scattering from a localized , cylindrically symmetric potential, Hamiltonian can be written as

$$\hat{H} = \begin{pmatrix} -\nabla^2 & -\kappa^2\beta_1\hat{k}_+ \\ -\kappa^2\beta_1\hat{k}_- & -\nabla^2 \end{pmatrix} \tag{2.20}$$

where $\nabla^2 = \frac{\partial^2}{\partial r^2} + \frac{1}{r}\frac{\partial}{\partial r} + \frac{1}{r^2}\frac{\partial^2}{\partial \varphi^2}$ and

$$\hat{k}_\pm = \hat{k}_x \pm i\hat{k}_y = -ie^{\pm i\varphi}(\frac{\partial}{\partial r} \pm \frac{i}{r}\frac{\partial}{\partial \varphi}) \quad . \tag{2.21}$$

The raising and lowering operators $\hat{k}_\pm$ work on Bessel function through the the recurrence relations

$$\begin{aligned} \wp_m'(z) + \tfrac{m}{z}\wp_m(z) &= \wp_{m-1}(z) \\ \wp_m'(z) - \tfrac{m}{z}\wp_m(z) &= -\wp_{m+1}(z) \end{aligned} \tag{2.22}$$

where $\wp$ denotes, Bessel function, Neumann function and Hankel function that we can get a relation

$$\hat{k}_\nu[J_m(\gamma r)e^{im\varphi}] = i\gamma\nu J_{m+\nu}(\gamma r)e^{i(m+\nu)\varphi} \quad (\nu = \pm) \quad . \tag{2.23}$$

The total Hamiltonian $\hat{H}$ commutes with the z projection of the total angular momentum

$$\hat{J}_z = L_z + \frac{1}{2}\sigma_z \tag{2.24}$$

that allows one to representation eigenstate of Eq. (2.20) as

$$\psi_m = \begin{pmatrix} A_m(r)e^{im\varphi} \\ B_{m'}(r)e^{im'\varphi} \end{pmatrix} \tag{2.25}$$

$A_m(r)$ and $B_{m'}(r)$ are both radial dependent , so we can make $A_m(r) = A^0 J_m(\gamma r)$ and $B_{m'}(r) = B^0 J_{m'}(\gamma r)$ $(m' = m-1)$ where A^0 and B^0 are arbitrary constants.

$$\psi_m = \begin{pmatrix} A^0 J_m(\gamma r)e^{im\varphi} \\ B^0 J_{m-1}(\gamma r)e^{i(m-1)\varphi} \end{pmatrix} \tag{2.26}$$

Substituting Eq. (2.23) into $\hat{H}\psi_m = \varepsilon\psi_m$, one can obtain the following systems of radial equations:

$$\begin{aligned} &\left(\{-\tfrac{1}{r}\tfrac{\partial}{\partial r}(r\tfrac{\partial}{\partial r}) + \tfrac{m^2}{r^2}\} - \left(\varepsilon + \kappa^2\beta_1 i\gamma\tfrac{B^0}{A^0}\right)\right) J_m(\gamma r) = 0 \quad , \\ &\left(\{-\tfrac{1}{r}\tfrac{\partial}{\partial r}(r\tfrac{\partial}{\partial r}) + \tfrac{(m-1)^2}{r^2}\} - \left(\varepsilon - \kappa^2\beta_1 i\gamma\tfrac{A^0}{B^0}\right)\right) J_{m-1}(\gamma r) = 0 \quad . \end{aligned} \tag{2.27}$$

The above equation must hold for the equation Eq. (2.28) due to the properties of Bessel function

$$\gamma^2 = \varepsilon + \kappa^2\beta_1 i\gamma\frac{B^0}{A^0} = \varepsilon - \kappa^2\beta_1 i\gamma\frac{A^0}{B^0} \tag{2.28}$$

To simplify our calculation, we define $R = \frac{B^0}{A^0}$. After calculation, we can get energy dispersion

$$\varepsilon = \gamma^2 + \eta\beta\gamma\kappa^2 \tag{2.29}$$

and the ratio R

$$R = \eta i \ (\eta = \pm) \ . \tag{2.30}$$

Consequently , the energy eigenstates of Hamiltonian with momentum γ, helicity η, and a ratio value $\Re$ are

$$\psi_{\eta m}(r, \varphi) = \begin{pmatrix} \Omega_{\eta m}(\gamma r) e^{im\varphi} \\ (\eta i)\Omega_{\eta(m-1)}(\gamma r) e^{i(m-1)\varphi} \end{pmatrix} \ , \tag{2.31}$$

where $\Omega_{\eta,m}$ can be a Bessel function, a Neumann function and a Hankel function. Here we choose Hankel functions as the eigenbasis to suit our boundary condition during the scattering process. The detail dervation of solving eigenequation is presented in appendix.

2.2 Cubic-k Dresselhaus SOI

2.2.1 Incident plane wave

The Hamiltonian for a 2DEG in the presence of the Dresselhaus SOI with a circular hard-wall disk at the origin can be expressed,

$$H = -\nabla^2 + \beta k_x(k_y^2 - \kappa^2)\sigma_x + \beta k_y(\kappa^2 - k_x^2)\sigma_y + V(\vec{r}) \tag{2.32}$$

where σ_j are the Pauli spin matrices and β is the Dresselhaus spin-orbit coupling constant . In order to distinct the contribution from the linear-k and cubic-k Dresselhaus SOI, we change the Hamiltonian form Eq. (2.32) into Eq. (2.33).

$$H = -\nabla^2 - \kappa^2\beta_1(k_x\sigma_x - k_y\sigma_y) + \beta_3(k_x k_y^2\sigma_x - k_y k_x^2\sigma_y) + V(\vec{r}) \tag{2.33}$$

where β_1 related to the linear-k Dresselhaus SOI and β_3 related to the cubic-k Dresselhaus SOI. The assumption for the scattering potential is same in the linear-k case (see Fig. 2.1).

The eigenstates and correspond eigenvalues for the free-particle Hamiltonian ($r \geq R$) with Dresselhaus spin-orbit coupling are given by

$$\psi_{in,\eta}(r,\varphi,\varphi_k) = e^{i\mathbf{k}\cdot\mathbf{r}}\chi_\eta \ , \tag{2.34}$$

$$\varepsilon = k^2 + \eta\beta_1 k\sqrt{\kappa^4 + [\frac{\beta_3}{2\beta_1}k^2\sin(2\varphi_k)]^2 - \frac{\beta_3}{\beta_1}k^2\kappa^2\sin^2(2\varphi_k)} \ , \tag{2.35}$$

where

$$\chi_\eta(\varphi_k) = \frac{1}{\sqrt{2}}\begin{pmatrix} 1 \\ R \end{pmatrix} = \frac{1}{\sqrt{2}}\begin{pmatrix} 1 \\ \eta\Re \end{pmatrix}, \tag{2.36}$$

$$\tan(\varphi_k) = \frac{k_y}{k_x},$$

$$R = \eta\Re \ , \tag{2.37}$$

and

$$\Re = -\sqrt{\frac{\kappa^2 e^{-i(\varphi_k)} + \frac{\beta_3}{2\beta_1}ik^2\sin(2\varphi_k)e^{i(\varphi_k)}}{\kappa^2 e^{i(\varphi_k)} - \frac{\beta_3}{2\beta_1}ik^2\sin(2\varphi_k)e^{-i(\varphi_k)}}} \ . \tag{2.38}$$

where $\Re$ denoting a ratio value which is function of incident angle and Dresselhaus SOI constant. The detail derivation of the eigenstates and eigenvalues shown in the appendix. The dispersion relation in Eq. (2.35) represents two helicity ($\eta = \pm$) branches.

For states propagating with their momentum vectors making an angle φ_k with respect to the $\hat{x}$ axis (see Fig. 2.3) and for an incident energy $E \geq 0$, there exits a degeneracy

with the degenerate with the degenerate states are given by

$$\psi_{in,+} = e^{i\mathbf{k}\cdot\mathbf{r}} \frac{1}{\sqrt{2}} \begin{pmatrix} 1 \\ \Re \end{pmatrix}, \tag{2.39}$$

$$\psi_{in,-} = e^{i\mathbf{k}'\cdot\mathbf{r}} \frac{1}{\sqrt{2}} \begin{pmatrix} 1 \\ -\Re \end{pmatrix}, \tag{2.40}$$

where $\overrightarrow{k} = k\left(\cos(\varphi_k)\hat{x} + \sin(\varphi_k)\hat{y}\right)$ and $\overrightarrow{k'} = k'\left(\cos(\varphi_k)\hat{x} + \sin(\varphi_k)\hat{y}\right)$ which you can obtain by solving

$$\varepsilon = k^2 + \beta_1 k \sqrt{\kappa^4 + [\frac{\beta_3}{2\beta_1} k^2 \sin(2\varphi_k)]^2 - \frac{\beta_3}{\beta_1} k^2 \kappa^2 \sin^2(2\varphi_k)} \tag{2.41}$$

and

$$\varepsilon = k'^2 - \beta_1 k' \sqrt{\kappa^4 + [\frac{\beta_3}{2\beta_1} k'^2 \sin(2\varphi_k)]^2 - \frac{\beta_3}{\beta_1} k'^2 \kappa^2 \sin^2(2\varphi_k)} \ . \tag{2.42}$$

The states Eq. (2.39) and Eq. (2.40) represent plane wave states with spin states shown in Eq. (2.36) being in the plane, perpendicular to the momentum direction. A plane wave corresponding to an free electron propagating with the momentum vector $\overrightarrow{k}$ making a propagating angle φ_k with $\hat{x}$ axis, in accordance with Jacobi-Anger expansion which can be expanded as a linear superposition of the circular free waves

$$e^{i\mathbf{kr}} = e^{ikr\cos(\varphi-\varphi_k)} = \sum_{m=-\infty}^{\infty} i^m J_m(kr) e^{im(\varphi-\varphi_k)} \ . \tag{2.43}$$

Then the incident plane wave with a specific momentum k and positive helicity ($\eta = +$)

Eq. (2.41) can be decomposed as the following linear superposition:

$$\psi_{in,+} = \frac{e^{i\mathbf{kr}}}{\sqrt{2}} \begin{pmatrix} 1 \\ \Re \end{pmatrix} = \frac{e^{ikr\cos(\varphi-\varphi_k)}}{\sqrt{2}} \begin{pmatrix} 1 \\ \Re \end{pmatrix} = \frac{1}{\sqrt{2}} \begin{pmatrix} \sum_m J_m(kr) e^{im(\varphi-\varphi_k)} \\ \sum_{m'} (\Re) J_{m'}(kr) e^{im'(\varphi-\varphi_k)} \end{pmatrix} \tag{2.44}$$

And then we can deal with cubic Dresselhaus SOI case in the same way just like plane wave in a linear Dresselhaus system.

Considering the scattering process with the cylindrical symmetric potential , we decompose Bessel function $J_m(kr)$ (**standing waves**) as Hankel functions $H_m^{(2)}(kr)$ (**incoming waves**) and $H_m^{(1)}(kr)$ (**outgoing waves**) so Eq. (2.45) become

$$\psi_{in,+} = \frac{1}{2\sqrt{2}} \sum_{m,m'=-\infty}^{\infty} \begin{pmatrix} i^m \left[H_m^{(2)}(kr) + H_m^{(1)}(kr) \right] e^{im(\varphi-\varphi_k)} \\ (\Re) i^{m'} \left[H_{m'}^{(2)}(kr) + H_{m'}^{(1)}(kr) \right] e^{im'(\varphi-\varphi_k)} \end{pmatrix}. \tag{2.45}$$

2.2.2 Cylindrical form representation of the eigenstates

In polar coordinates, which are useful when we consider scattering from a localized, cylindrically symmetric potential ($hard - wall\ disk$), Hamiltonian can be written as

$$\hat{H} = \begin{pmatrix} -\nabla^2 & -\kappa^2\beta_1\hat{k}_+ + \frac{\beta_3}{4}(\hat{k}_+^2 - \hat{k}_-^2)\hat{k}_- \\ -\kappa^2\beta_1\hat{k}_- - \frac{\beta_3}{4}(\hat{k}_+^2 - \hat{k}_-^2)\hat{k}_+ & -\nabla^2 \end{pmatrix} \tag{2.46}$$

where $\nabla^2 = \frac{\partial^2}{\partial r^2} + \frac{1}{r}\frac{\partial}{\partial r} + \frac{1}{r^2}\frac{\partial^2}{\partial \varphi^2}$ and

$$\hat{k}_\pm = \hat{k}_x \pm i\hat{k}_y = -ie^{\pm i\varphi}\left(\frac{\partial}{\partial r} \pm \frac{i}{r}\frac{\partial}{\partial \varphi}\right) \tag{2.47}$$

For solving the eigenequation $\hat{H}\psi = \varepsilon\psi$ in a localized and cylindrically symmetric

potential, the eigenstates can be written as a two-component wave function.

$$\psi(r,\varphi) = \begin{pmatrix} \sum_m A_m(r)e^{im\varphi} \\ \sum_{m'} B_{m'}(r)e^{im'\varphi} \end{pmatrix} \tag{2.48}$$

Since $A_m(r)$ and $B_{m'}(r)$ both have radial-dependence, we assume that $A_m(r) = A^0_m J_m(\gamma r)$ and $B_{m'}(r) = B^0_{m'} J_{m'}(\gamma r)$. Then wavefunction become a two-component function which is a linear superposition of Bessel functions

$$\psi(r,\varphi) = \begin{pmatrix} \sum_m A^0_m J_m(\gamma r)e^{im\varphi} \\ \sum_{m'} B^0_{m'} J_{m'}(\gamma r)e^{im'\varphi} \end{pmatrix} \tag{2.49}$$

where A^0_m and $B^0_{m'}$ are unknown constants which are determined by eigenequations. And then we can deal with cubic-k Dresselhaus SOI case in the same way similar to plane wave in a linear-k Dresselhaus system.

$$\hat{k}_\nu[J_m(\gamma r)e^{im\varphi}] = i\gamma\nu J_{m+\nu}(\gamma r)e^{i(m+\nu)\varphi} \quad (\nu = \pm) \quad . \tag{2.50}$$

Substituting Eq. (2.49) and Eq. (2.50) into equation $\hat{H}\psi = \varepsilon\psi$, one can obtain the following radial equations:

$$\begin{aligned} &\{-\tfrac{1}{r}\tfrac{\partial}{\partial r}(r\tfrac{\partial}{\partial r}) + \tfrac{m^2}{r^2} - (\varepsilon + \kappa^2\beta_1\gamma i\tfrac{B^0_{m-1}}{A^0_m} - i\tfrac{\beta_3}{4}\gamma^3\tfrac{B^0_{m-1}}{A^0_m} + i\tfrac{\beta_3}{4}\gamma^3\tfrac{B^0_{m+3}}{A^0_m})\}J_m(\gamma r) = 0, \\ &\{-\tfrac{1}{r}\tfrac{\partial}{\partial r}(r\tfrac{\partial}{\partial r}) + \tfrac{m^2}{r^2} - (\varepsilon - \kappa^2\beta_1 i\gamma\tfrac{A^0_{m+1}}{B^0_m} - i\tfrac{\beta_3}{4}\gamma^3\tfrac{A^0_{m-3}}{B^0_m} + i\tfrac{\beta_3}{4}\gamma^3\tfrac{A^0_{m+1}}{B^0_m})\}J_m(\gamma r) = 0. \end{aligned} \tag{2.51}$$

By setting

$$A^0_m \sim A^0 x^m \quad , \quad B^0_m \sim B^0 x^m \tag{2.52}$$

and using properties of Bessel functions, gives rise to Eq. (2.51)

$$\begin{aligned}&(\varepsilon+\kappa^2\beta_1\gamma i\tfrac{B^0}{A^0}x^{-1}-i\tfrac{\beta_3}{4}\gamma^3\tfrac{B^0}{A^0}x^{-1}+i\tfrac{\beta_3}{4}\gamma^3\tfrac{B^0}{A^0}x^3)\\&=(\varepsilon-\kappa^2\beta_1 i\gamma\tfrac{A^0}{B^0}x-i\tfrac{\beta_3}{4}\gamma^3\tfrac{A^0}{B^0}x^{-3}+i\tfrac{\beta_3}{4}\gamma^3\tfrac{A^0}{B^0}x)\\&=\gamma^2\quad.\end{aligned}\tag{2.53}$$

To simplify our calculations, we let $R=B^0/A^0$. We also assume that $R{=}e^{i\theta}$ and $x=e^{i\delta}$ are both phase vectors. As a result, we obtain two simple relations

$$\begin{aligned}&\varepsilon+e^{i(\theta+\delta)}\beta_1\gamma(i\kappa^2e^{-i2\delta}-\tfrac{\beta_3}{\beta_1}\tfrac{\gamma^2}{2}\sin(2\delta))\\&=\varepsilon-e^{-i(\theta+\delta)}\beta_1\gamma(i\kappa^2e^{i2\delta}+\tfrac{\beta_3}{\beta_1}\tfrac{\gamma^2}{2}\sin(2\delta))\\&=\gamma^2\end{aligned}\tag{2.54}$$

between momentum γ and energy ε . From Eq. (2.54), the unknown values can be solved. The eigenstate is

$$\psi_\eta(r,\varphi)=\begin{pmatrix}\sum_m J_m(\gamma r)e^{im\varphi}e^{im\delta}\\ \sum_{m'}(\eta\Re)J_{m'}(\gamma r)e^{im'\varphi}e^{im'\delta}\end{pmatrix}\tag{2.55}$$

where

$$\Re=e^{-i\delta}\sqrt{-\frac{(i\kappa^2e^{i2\delta}+\frac{\beta_3}{\beta_1}\frac{\gamma^2}{2}\sin(2\delta))}{(i\kappa^2e^{-i2\delta}-\frac{\beta_3}{\beta_1}\frac{\gamma^2}{2}\sin(2\delta))}}\tag{2.56}$$

and eigenenergy is

$$\varepsilon=\gamma^2+\eta\beta_1\gamma\sqrt{\kappa^4+(\frac{\beta_3}{\beta_1}\frac{\gamma^2}{2})^2\sin^2(2\delta)-\kappa^2\frac{\beta_3}{\beta_1}\gamma^2\sin^2(2\delta)}\quad.\tag{2.57}$$

Here $\eta=\pm$ can be viewed as helicity $+$ and helicity $-$. Consequently , the energy eigenstates of Hamiltonian Eq. (2.46) with momentum γ, a phase δ, helicity η, and a

ratio value $\Re$ are

$$\psi_\eta(r,\varphi) = \begin{pmatrix} \sum_m \Omega_m(\gamma r)e^{im\varphi}e^{im\delta} \\ \sum_{m'} (\eta\Re)\Omega_{m'}(\gamma r)e^{im'\varphi}e^{im'\delta} \end{pmatrix} \tag{2.58}$$

where Ω can be a Bessel function, a Neumann function and a Hankel function. Here we choose Hankel functions as the eigenbasis to suit our boundary condition at infinity during the scattering process. The detail derivation of solving eigenequation is presented in Appendix.

2.3 Energy dispersion of Dresselhaus SOI system

In this section, we discuss the energy dispersion of Dresselhaus SOI system including linear and cubic k. For given energy dispersions from the Eq. (2.5) and Eq. (2.35), we find that the energy dispersion in cubic k DSOI system Eq. (2.35) which is dependent on the incident angle φ_k. As a result, we propose energy dispersion diagrams in different scales which are given by Fig. 2.4 and Fig. 2.5. On the other hand, the energy dispersion in linear k DSOI system

$$\varepsilon = k^2 \pm (\beta\kappa^2)k$$

is like in the RSOI system

$$\varepsilon = k^2 \pm \alpha k$$

but the spin orbit couple strength in the later case is stronger ($\alpha \gg \tilde{\beta} = \beta\kappa^2$)

$$\frac{\beta\kappa^2}{\alpha} = \frac{\left(27\text{eVA}^3\right)\left(0.209\text{nm }\right)^2}{0.35\text{nmeV}} \cong 0.003 \ .$$

The twofold denervate branch ($\eta = \pm$) is unapparent due to the small k contribution that we found from Fig. 2.4. In contrast, the degeneration is more apparent in Fig. 2.5 if k becomes larger gradually in the larger k range. In the specific incident plane angle Eq. (2.35) is reduced to Eq. (2.5). We can use the special cases to know what differential contribution from linear and cubic k although the cubic k contribution is smaller. At the same time, the DSOI linear k result can be compared with the RSOI result [16].

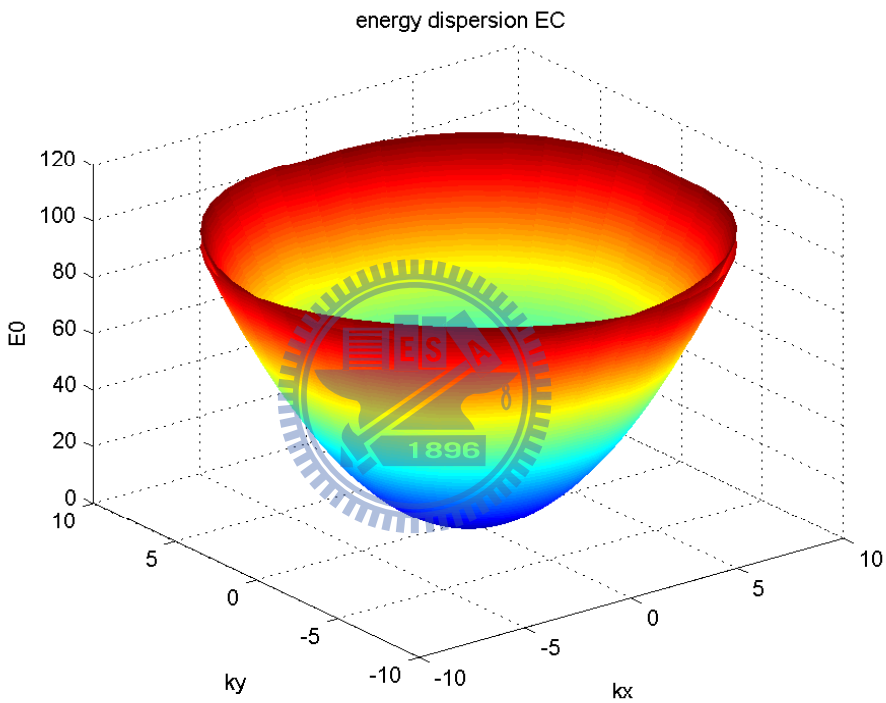

Figure 2.4: Dispersion relation for a 2D Dresselhaus-type system (includes linear and cubic terms) and the Dresselhaus constant $\beta = 27\text{eV}\,\mathring{A}^3$ and $d = 15nm$.

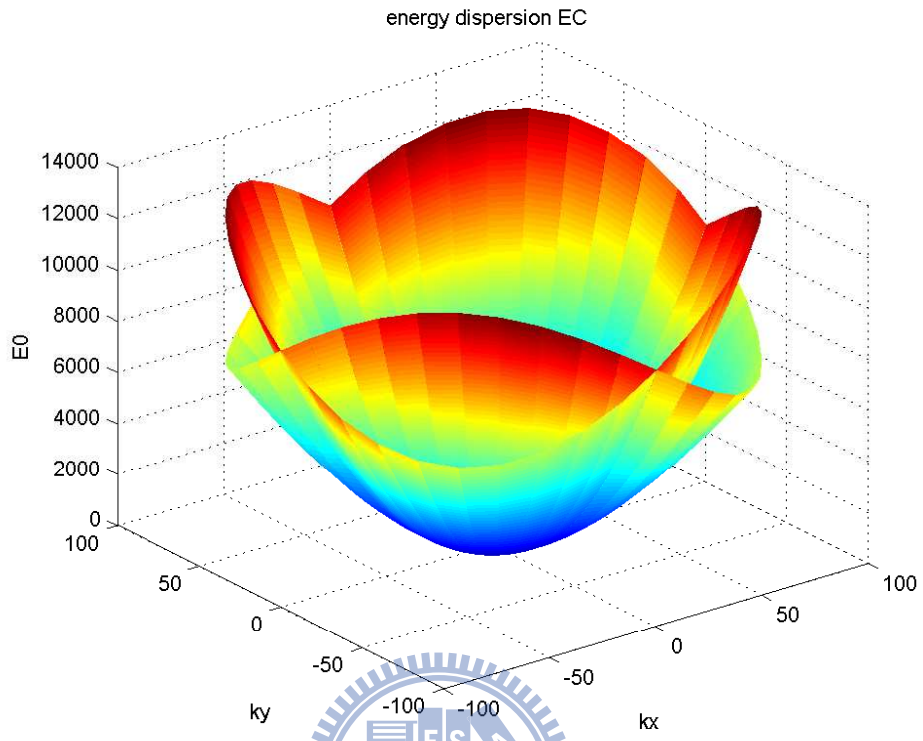

Figure 2.5: Dispersion relation for a 2D Dresselhaus-type system (includes linear and cubic terms) and the Dresselhaus constant $\beta = 27\text{eV}\,\text{Å}^3$ and $d = 15nm$ in the larger k range.

On the other hand, we obtain three roots by solving the energy dispersion in cubic-k system Eq. (2.35) for a given energy ε and incident angle φ_k. For the example, the incident angle φ_k is $\frac{\pi}{3}$ and the helicity is positive so that we can evaluate the roots of the energy dispersion in Fig. 2.6.

The roots of the energy dispersion Eq. (2.35) where $\varphi_k = \frac{\pi}{3}$ and $\eta = +$. The right pattern is the real part of k and the left pattern is the imagine part of k. In the central region of the real k and k imagine pattern show that the three roots in the region are all pure real values. Apparently, the momentum k we have to neglect is only the smallest one due to the corresponding much fast oscillation and then the others are exactly we must consider. By the way, the energy ε in the top and bottom regions of the real k and imagine k pattern are not the incident energy so that here we don't discuss them. Similarly, if the energy

dispersion has negative helicity, we also can use the manner to obtain the momentums in the same way. The smaller pattern of Fig. 2.6 is the energy dispersion of the incident plane wave where the incident energy ε which we consider is located in the energy region. But just like the energy dispersion

$$\varepsilon = k^2 + \eta\beta_1 k\sqrt{\kappa^4 + [\frac{\beta_3}{2\beta_1}k^2\sin(2\varphi_k)]^2 - \frac{\beta_3}{\beta_1}k^2\kappa^2\sin^2(2\varphi_k)}$$

we have derived before, the incident wave angle φ_k can determine the number of roots of the energy dispersion. However, the roots of the energy dispersion in linear-k DSOI system Eq. (2.5) or in cubic-k DSOIsystermEq. (2.35) we need are both two roots.

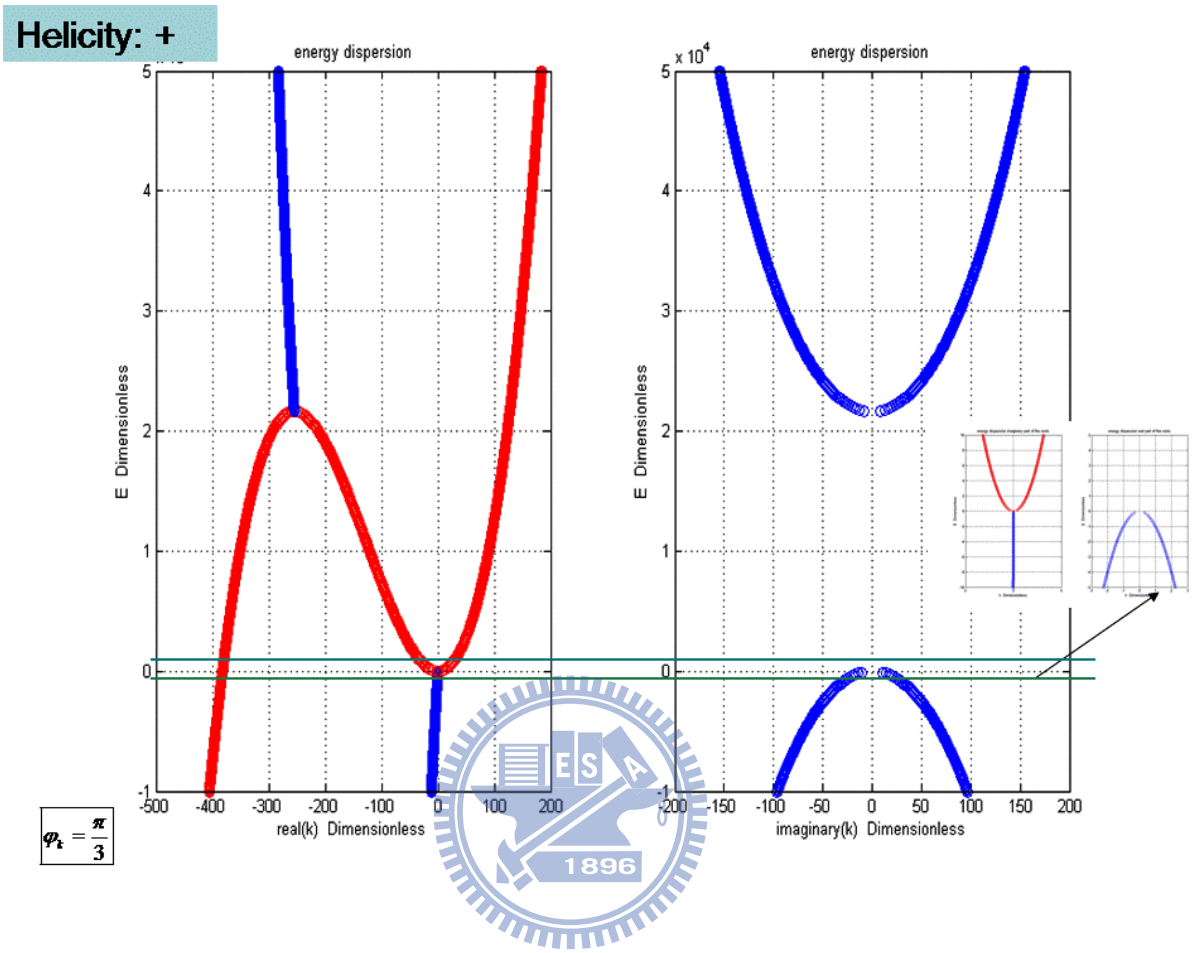

Figure 2.6: The roots of the energy dispersion Eq. (2.35) where $\varphi_k = \frac{\pi}{3}$ and $\eta = +$. The right pattern is the real part of k and the left pattern is the imagine part of k. In the central region of the real k and k imagine pattern show that the three roots in the region are all pure real values. Apparently, the momentum k we have to neglect is only the smallest one due to the corresponding much fast oscillation and then the others are exactly we must consider.

2.4 BIA in spin splitting in 2D systems

For two dimension systems,we can estimate the BIA-induced spin splitting. We obtain a spin splitting

$$\Delta\varepsilon(\vec{k}) = \pm\beta_1 k\sqrt{\kappa^4 + [\frac{\beta_3}{2\beta_1}k^2\sin(2\varphi_k)]^2 - \frac{\beta_3}{\beta_1}k^2\kappa^2\sin^2(2\varphi_k)} \tag{2.59}$$

To reduce the energy splitting form Eq. (2.59), we make Dresselhaus constant return

to the origin shape ($\beta_1 = \beta_3 = \beta$) and Eq. (2.59) becomes

$$\Delta\varepsilon(\mathbf{k}) = \pm\beta k\sqrt{\kappa^4 + [\frac{1}{4}k^2 - \kappa^2]k^2\sin^2(2\varphi_k)} \tag{2.60a}$$

$$\approx \pm\beta\left[\kappa^2k^2 - \frac{1}{2}\kappa^3\sin^2(2\varphi_k) + \eth\left(k^5\right)\right]. \tag{2.60b}$$

where $\vec{k} = k\cos(\varphi_k)\hat{x} + k\sin(\varphi_k)\hat{y}$. We have used κ to replace with the expectation value $\langle k_z\rangle$ of the wave vector along z-direction. For small $\vec{k}$ the BIA spin splitting is linear in $\vec{k}$ and independent of the direction of $\vec{k}$. For larger values of $\vec{k}$ the BIA spin splitting becomes anisotropic, with energy surfaces that have a fourfold rotational symmetry. Note also that for $\varphi_k = 0\left(\vec{k} \parallel [100]\right)$ and $\varphi_k = \frac{\pi}{4}\left(\vec{k} \parallel [110]\right)$, Eq. (2.60) is exact [2]. Within our approach we thus have zero BIA spin splitting for $\varphi_k = \frac{\pi}{4}$ and $k^2 = 2\kappa^2$.

2.5 Connection between linear-k DSOI and ROSI systems

For a 2DEG system, linear-k DSOI Hamiltonian is like RSOI Hamiltonian. We can make a coordinate rotation about DSOI Hamiltonian

$$H_D = \beta\ (\sigma_x k_x - \sigma_y k_y) \tag{2.61}$$

and then the rotated DSOI Hamiltonian to compare with RSOI Hamiltonian

$$H_R = \alpha(\sigma_x k_y - \sigma_y k_x) \tag{2.62}$$

where α is the Rashba spin orbiting constant and β is the Dresselhaus spin orbiting constants. Suppose, for instance, the $[x', y']$ system is rotated by angle θ Fig. 2.7, relative to the $[x, y]$ system. After calculation, we might express the relation between $[x', y']$

system and $[x, y]$ system in matrix notation:

$$\begin{pmatrix} x' \\ y' \end{pmatrix} = \begin{pmatrix} \cos(\theta) & \sin(\theta) \\ -\sin(\theta) & \cos(\theta) \end{pmatrix} \begin{pmatrix} x \\ y \end{pmatrix} \quad . \tag{2.63}$$

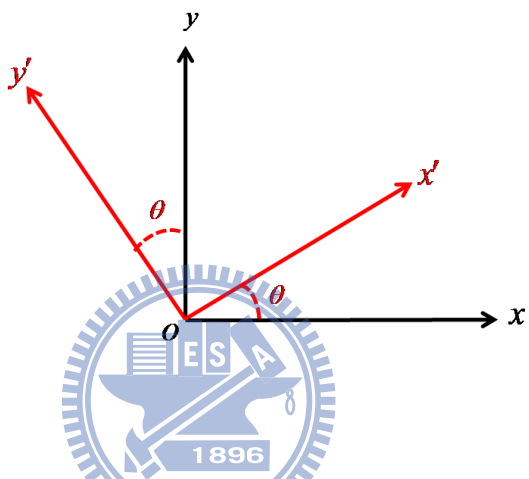

Figure 2.7: the $[x', y']$ system is rotated by angle θ, retaliative to the $[x, y]$ system.

In the same way, Dresselhaus type Hamiltonian in $[x', y']$ system is

$$H'_D = \beta\left(k_{x'}\sigma_{x'} - k_{y'}\sigma_{y'}\right)$$

and then it is transformed into $[x', y']$ system after coordinate rotation. Similar to Eq. (2.63), we can use the same rotation matrix in momentum $k_{x'}(k_{y'})$ and Pauli matrix $\sigma_{x'}(\sigma_{x'})$. The detailed derivation of the coordinate rotation between linear-k DSOI and RSOI Hamiltonians are shown in the appendix. After a coordinate rotation, the linear-k DSOI Hamiltonian in $[x, y]$ system is given by

$$H'_D(\theta) = H_D = \beta\left(k_x\sigma_x - k_y\sigma_y\right)\cos(2\theta) + \beta\left(k_x\sigma_y + k_y\sigma_x\right)\sin(2\theta) \quad . \tag{2.64}$$

We can chose a special rotating angle $\frac{\pi}{4}$ and then the corresponding rotated Hamiltonian

$$H'_D(\frac{\pi}{4}) = H_D = \beta\left(k_x\sigma_y + k_y\sigma_x\right) \tag{2.65}$$

is like ROI Hamiltonian Eq. (2.62) so that we can make a competition between them. It means that the propagating with their momentum k making a angle $\varphi_k = \frac{\pi}{4}$ with respect to the $\hat{x}$ axis in linear k Dresselhaus SOI system whose propagating process is compellable. We can discuss the spin density or the probability density distribution in this case comparing the Rashba result.

Chapter 3

Scattering from a cylindrically symmetric potential in a Dresselhaus SOI system

The main focus in this chapter is discussed the scattering process. We first present the spin dependent scattering calculation including cylindrical wave representations of the incoming wave and the outgoing wave and then for a given m these equations involving Hankel functions can be transformed into a $m \times m$ matrices result from independence of the angle. We can determine the unknown coefficients by solving this boundary condition problem.

In contrast, the scattering process in linear-k DSOI system can be solved analytically so that the total function and the spin density both have analytical forms. The spin density distribution is evaluated exactly and it is helpful to analyze the cubic-k DSOI case. For a given total wave function, spin density will be studies. Finally, we drive particle continuity equation in Dresselhaus SOI Hamiltonian to find the particle current.

3.1 Cubic-k Dresselhaus SOI

3.1.1 Coupled cylindrical wave representations of the incoming wave

First, we choose the propagating direction of the incident plane wave along $\hat{x}$-direction with the angle φ_k respecting to the $\hat{x}$ axis in Drsselhaus-type SOI system. Then, in cylindrical coordinate, incident plane wave with the incident energy ε, a ratio $\Re$, momentum γ and helicity $\eta = +$ can be expansion of partial waves

$$\psi_{\text{incoming}} = \frac{1}{2\sqrt{2}} \sum_{m,m'=-\infty}^{\infty} \begin{pmatrix} i^m H_m^{(2)}(\gamma r) e^{im(\varphi-\varphi_k)} \\ \Re_{inc} i^{m'} H_{m'}^{(2)}(\gamma r) e^{im'(\varphi-\varphi_k)} \end{pmatrix}. \tag{3.1}$$

For the scattering process in the Dresselhaus-type system we can take ψ as a eigenbasis

$$\psi = A \begin{pmatrix} \sum_m J_m(\gamma r) e^{im\varphi} e^{im\delta} \\ \sum_{m'} (\eta\Re) J_{m'}(\gamma r) e^{im'\varphi} e^{im'\delta} \end{pmatrix} \tag{3.2}$$

where

$$\Re = e^{-i\delta} \sqrt{-\frac{(i\kappa^2 e^{i2\delta} + \frac{\beta_3}{\beta_1}\frac{\gamma^2}{2}\sin(2\delta))}{(i\kappa^2 e^{-i2\delta} - \frac{\beta_3}{\beta_1}\frac{\gamma^2}{2}\sin(2\delta))}} \tag{3.3}$$

, A is a unknown constant and

$$\varepsilon = \gamma^2 + \eta\beta_1\gamma\sqrt{\kappa^4 + (\frac{\beta_3}{\beta_1}\frac{\gamma^2}{2})^2 \sin^2(2\delta) - \kappa^2\frac{\beta_3}{\beta_1}\gamma^2 \sin^2(2\delta)}. \tag{3.4}$$

due to the central cylindrical symmetric potential.

The total wave function outside the scattering region ($r > R$) has the form

$$\psi_{total} = \psi_{outgoing} + \psi_{\text{incoming}} \tag{3.5}$$

where

$$\psi_{\text{incoming}} = c \begin{pmatrix} g_1(\gamma, \mathbf{r}, \delta) \\ g_2(\gamma, \mathbf{r}, \delta) \end{pmatrix} \tag{3.6}$$

and

$$\psi_{outgoing} = \int_0^{2\pi} d\delta a(\delta) \begin{pmatrix} f_1(\gamma, \mathbf{r}, \delta) \\ f_2(\gamma, \mathbf{r}, \delta) \end{pmatrix} + \int_0^{2\pi} d\delta' b(\delta') \begin{pmatrix} f_1(\gamma', \mathbf{r}, \delta') \\ f_2(\gamma', \mathbf{r}, \delta') \end{pmatrix} . \tag{3.7}$$

(postive helicity : γ , δ negative helicity : γ' , δ')

Here $f_1(f_2)$ are the first kind Hankel functions and $g_1(g_2)$ are the second kind Hankel functions. From Eq. (3.5) to Eq. (3.7), it can show that if an incident wave has a specific helicity $\psi_{in,+}$, no incoming cylindrical wave with negative helicity and nonzero coefficient $b(\delta')$ lead to outgoing waves with flipped helicity (outgoing wave must have both $\eta = \pm$). For a given incident plane wave Eq. (3.1), we look at the incoming part that the all coefficients in Eq. (3.6) can be determined and use $\Re_{inc}$ to replace with $\Re$ where $\Re_{inc}$ is a function of φ_k in order to avoid to confuse the incoming wave with the outgoing wave.

$$\psi_{\text{incoming}} = \frac{1}{2\sqrt{2}} \sum_{m,m'=-\infty}^{\infty} \begin{pmatrix} i^m H_m^{(2)}(\gamma r) e^{im(\varphi-\varphi_k)} \\ \Re_{inc} i^{m'} H_{m'}^{(2)}(\gamma r) e^{im'(\varphi-\varphi_k)} \end{pmatrix} \tag{3.8}$$

$$\varepsilon = \gamma^2 + \beta_1 \gamma \sqrt{\kappa^4 + [\frac{\beta_3}{2\beta_1}\gamma^2 \sin(2\varphi_k)]^2 - \frac{\beta_3}{\beta_1}\gamma^2\kappa^2 \sin^2(2\varphi_k)} \tag{3.9}$$

$$\Re_{inc} = -\sqrt{\frac{\kappa^2 e^{-i(\varphi_k)} + \frac{\beta_3}{2\beta_1} i\gamma^2 \sin(2\varphi_k) e^{i(\varphi_k)}}{\kappa^2 e^{i(\varphi_k)} - \frac{\beta_3}{2\beta_1} i\gamma^2 \sin(2\varphi_k) e^{-i(\varphi_k)}}} \tag{3.10}$$

Boundary conditions will be established in the later section for the solving of unknown coefficients of outgoing wave Eq. (3.7). And we simplify the outgoing wave part in the next section.

3.1.2 Coupled cylindrical wave representations of the outgoing wave

The continuous integration $\int_0^{2\pi} d\delta$ in Eq. (3.7) can be treated as the discrete summation $\sum_{i=1}^{N} \Delta\delta$ in representation of a matrix form to and then use it to solve the boundary problem in the numerical method. Here δ describes that the integration range of δ from 0 to 2π is divided into N pieces and each piece $\Delta\delta = 2\pi/N$. The summation is more close to the integration if N is larger enough. In the later section, we can determine N through the numerical result of the spin density and the probability of the total wave function.

The integration approximation is estimated by

$$\int_0^{2\pi} d\delta \rightarrow \sum_{i=1}^{N} \Delta\delta \quad \text{and} \quad \int_0^{2\pi} d\delta' \rightarrow \sum_{i=1}^{N} \Delta\delta' \tag{3.11}$$

The outgoing wave part of the total wave function Eq. (3.7) can be regarded as the discrete form

$$\psi_{outgoing} = \sum_{n=1}^{N} \Delta\delta a(\delta_n) \begin{pmatrix} f_1(\gamma_n, \mathbf{r}, \delta_n) \\ f_2(\gamma_n, \mathbf{r}, \delta_n) \end{pmatrix} + \sum_{n=1}^{N} \Delta\delta' b(\delta_n) \begin{pmatrix} f_1(\gamma'_n, \mathbf{r}, \delta'_n) \\ f_2(\gamma'_n, \mathbf{r}, \delta'_n) \end{pmatrix} \tag{3.12}$$

where $\Delta\delta = \frac{2\pi}{N} = \Delta\delta'$ and $\delta_n = n\Delta\delta = n\Delta\delta' = \delta'_n$. The unknown constants $a(\delta_n)$ and $b(\delta_n)$ are function of δ_n and then δ_n is the Nth piece of the angle δ. Substituting the eigenbasis Eq. (3.2) into the Eq. (3.12), we have the outgoing wave function in the discrete form

$$\begin{aligned} \psi_{outgoing} = & \sum_{n=1}^{N} \Delta\delta a(\delta_n) \begin{pmatrix} \sum_{m=-\infty}^{\infty} H_m^{(1)}(\gamma_n r) e^{im(\varphi+\delta_n)} \\ (\Re_n) \sum_{m'=-\infty}^{\infty} H_{m'}^{(1)}(\gamma_n r) e^{im'(\varphi+\delta_n)} \end{pmatrix} \\ & + \sum_{n=1}^{N} \Delta\delta' b(\delta'_n) \begin{pmatrix} \sum_{m=-\infty}^{\infty} H_m^{(1)}(\gamma'_n r) e^{im(\varphi+\delta'_n)} \\ (\Re'_n) \sum_{m'=-\infty}^{\infty} H_{m'}^{(1)}(\gamma'_n r) e^{im'(\varphi+\delta'_n)} \end{pmatrix} \end{aligned} \tag{3.13}$$

The equation shows that consider a incident plane wave with positive helicity after scattering by central symmetric potential (hard wall disk) whose incoming wave part is the same as before scattering but the outgoing wave part including both positive and negative helicity lead to spin flipping. For a reference, if the incident wave has only negative helicity, then the helicity of the incoming wave part is still negative. At the same time, the rules of γ and γ', as well as the probability amplitudes $a(\delta)$ and $b(\delta')$ must be interchanged.

We can easily deduce the outgoing wave function into the convenient form with the representation $a_m(\delta_n) = a_m$ and $b_{m'}(\delta_n) = b_{m'}$ and then it becomes

$$\psi_{outgoing} = \sum_{n=1}^{N} \Delta\delta \begin{pmatrix} \sum\limits_{m=-\infty}^{\infty} [a_n H_m^{(1)}(\gamma_n r) e^{im(\varphi+\delta_n)} + b_n H_m^{(1)}(\gamma_n' r) e^{im(\varphi+\delta_n)}] \\ \sum\limits_{m'=-\infty}^{\infty} [a_n(\Re_n) H_{m'}^{(1)}(\gamma_n r) e^{im'(\varphi+\delta_n)} + b_n(\Re_n') H_{m'}^{(1)}(\gamma_n' r) e^{im'(\varphi+\delta_n)}] \end{pmatrix} \tag{3.14}$$

Here the correspond energy dispersion and the ratio are

$$\varepsilon = \gamma_n^2 + \beta_1\gamma_n \sqrt{\kappa^4 + (\frac{\beta_3}{\beta_1}\frac{\gamma_n^2}{2})^2 \sin^2(2\delta_n) - \kappa^2 \frac{\beta_3}{\beta_1}\gamma_n^2 \sin^2(2\delta_n)} \quad , \tag{3.15}$$

$$\Re_n = e^{-i\delta_n} \sqrt{-\frac{(i\kappa^2 e^{i2\delta_n} + \frac{\beta_3}{\beta_1}\frac{\gamma_n^2}{2}\sin(2\delta_n))}{(i\kappa^2 e^{-i2\delta_n} - \frac{\beta_3}{\beta_1}\frac{\gamma_n^2}{2}\sin(2\delta_n))}} \tag{3.16}$$

and

$$\varepsilon = (\gamma_n')^2 - \beta_1\gamma_n' \sqrt{\kappa^4 + (\frac{\beta_3}{\beta_1}\frac{(\gamma_n')^2}{2})^2 \sin^2(2\delta_n) - \kappa^2 \frac{\beta_3}{\beta_1}(\gamma_n')^2 \sin^2(2\delta_n)} \quad , \tag{3.17}$$

$$\Re_n' = -e^{-i\delta_n} \sqrt{-\frac{(i\kappa^2 e^{i2\delta_n} + \frac{\beta_3}{\beta_1}\frac{(\gamma_n')^2}{2}\sin(2\delta_n))}{(i\kappa^2 e^{-i2\delta_n} - \frac{\beta_3}{\beta_1}\frac{(\gamma_n')^2}{2}\sin(2\delta_n))}} \tag{3.18}$$

; Eq. (3.15) and Eq. (3.16) corresponding to helicity $\eta = +$, while Eq. (3.17) and Eq. (3.18) correspond to $\eta = -$. In the case of helicity $\eta = +$, for a given energy ε, momentum γ_n can be get from the energy dispersion in each δ_n. And then if momentum is known, we also obtain the correspond ratio $\Re_n$ by solving the equation which is function of η and δ_n Eq. (3.16). The negative helicity case is the same as the negative helicity case , so all parameters is known for a given energy expect for the probability a_n and b_n which we can determine by the boundary condition. After detailed calculation process in **section** 3.1 and this section, from the incoming wave part in Eq. (3.8) and the outgoing wave part in Eq. (3.14), the total wave function with the incident angle φ_k outside the disk Eq. (3.5) is given by

$$\psi_{total}(r,\varphi,\varphi_k) = \begin{pmatrix} \sum_{n=1}^{N}\sum_{m=-\infty}^{\infty}\Delta\delta[a_n H_m^{(1)}(\gamma_n r)e^{im(\varphi+\delta_n)} + b_n H_m^{(1)}(\gamma_n' r)e^{im(\varphi+\delta_n)}] \\ + \frac{1}{2\sqrt{2}}\sum_{m=-\infty}^{\infty} i^m H_m^{(2)}(\gamma r)e^{im(\varphi-\varphi_k)} \\ \sum_{n=1}^{N}\sum_{m'=-\infty}^{\infty}\Delta\delta[a_n(\Re_n)H_{m'}^{(1)}(\gamma_n r)e^{im'(\varphi+\delta_n)} + b_n(\Re_n')H_{m'}^{(1)}(\gamma_n' r)e^{im'(\varphi+\delta_n)}] \\ + \frac{1}{2\sqrt{2}}\sum_{m'=-\infty}^{\infty}(\Re_{inc})i^{m'}H_{m'}^{(2)}(\gamma r)e^{im'(\varphi-\varphi_k)} \end{pmatrix} \tag{3.19}$$

The total wave function φ_k outside the scattering region ($r \geq R$) for a given incident angle must be zero which is independent of the angle φ at $r = R$ due to the boundary condition of the cental symmetric potential ("hard " wall disk).

$$\psi_{total}(R,\varphi,\varphi_k) = \begin{pmatrix} \sum_{n=1}^{N}\sum_{m=-\infty}^{\infty}\Delta\delta[a_n H_m^{(1)}(\gamma_n R)e^{im(\varphi+\delta_n)} + b_n H_m^{(1)}(\gamma_n' R)e^{im(\varphi+\delta_n)}] \\ + \frac{1}{2\sqrt{2}}\sum_{m=-\infty}^{\infty} i^m H_m^{(2)}(\gamma R)e^{im(\varphi-\varphi_k)} \\ \sum_{n=1}^{N}\sum_{m'=-\infty}^{\infty}\Delta\delta[a_n(\Re_n)H_{m'}^{(1)}(\gamma_n R)e^{im'(\varphi+\delta_n)} + b_n(\Re_n')H_{m'}^{(1)}(\gamma_n' R)e^{im'(\varphi+\delta_n)}] \\ + \frac{1}{2\sqrt{2}}\sum_{m'=-\infty}^{\infty}(\Re_{inc})i^{m'}H_{m'}^{(2)}(\gamma R)e^{im'(\varphi-\varphi_k)} \end{pmatrix}$$

$$= 0$$

(3.20)

In Eq. (3.20) the summation $\sum_{m=-\infty}^{\infty}$ we can define a finite range from $-m$ to m to represent an infinite range just like Eq. (3.11) . At the same time, we make N in Eq. (3.11) equal $2M+1$ so that the first low of the total wave function is given by

$$\sum_{m=-M}^{M}\left(\sum_{n=1}^{2M+1}\Delta\delta e^{im(\varphi+\delta_n)}[a_n f_{mn}+b_n f'_{mn}]+g_m e^{im(\varphi-\varphi_k)}\right) \tag{3.21}$$

where $f_{mn}=H_m^{(1)}(\gamma_n R)$, $f'_{mn}=H_m^{(1)}(\gamma'_n R)$ and $g_m=\frac{i^m}{2\sqrt{2}}H_m^{(2)}(\gamma R)$.
And each piece $\Delta\delta$ is equal to $\frac{2\pi}{2M+1}$ corresponding $\delta_n=n\Delta\delta=n\frac{2\pi}{2M+1}$. In the same way, the second low has the similar form

$$\sum_{m'=-M}^{M}\left(\sum_{n=1}^{2M+1}\Delta\delta e^{im'(\varphi+\delta_n)}[a_n(\Re_n)f_{m'n}+b_n(\Re'_n)f'_{m'n}]+(\Re_{inc})g_{m'}e^{im'(\varphi-\varphi_k)}\right) \tag{3.22}$$

where $e^{i\theta_n}f_{m'n}=(\Re_n)H_{m'}^{(1)}(\gamma_n R)$, $e^{i\theta'_n}f'_{m'n}=(\Re'_n)H_{m'}^{(1)}(\gamma'_n R)$ and $g_{m'}=\frac{i^{m'}}{2\sqrt{2}}H_{m'}^{(2)}(\gamma R)$. Then the total wave functions on the bound $(r=R)$ reduce to a simply form as following

$$\psi_{total}(R,\varphi,\varphi_k) = \begin{pmatrix} \sum_{m=-M}^{M}\left(\sum_{n=1}^{2M+1}\Delta\delta e^{im(\varphi+\delta_n)}[a_n f_{mn}+b_n f'_{mn}]+g_m e^{im(\varphi-\varphi_k)}\right) \\ \sum_{m'=-M}^{M}\left(\sum_{n=1}^{2M+1}\Delta\delta e^{im'(\varphi+\delta_n)}[a_n(\Re_n)f_{m'n}+b_n(\Re'_n)f'_{m'n}]+(\Re_{inc})g_{m'}e^{im'(\varphi-\varphi_k)}\right) \end{pmatrix} = 0 \ . \tag{3.23}$$

We use the orthogonal relation on the summations of the two component matrix since the "hard" wall boundary is φ independent. Taking into the orthogonal relation on φ, the first low Eq. (3.21) have no φ dependence, we have

$$\sum_{n=1}^{2M+1}\left(e^{im''\delta_n}[f_{m''n}a_n+f'_{m''n}b_n]\right)=-\frac{1}{\Delta\delta}G_{m''} \tag{3.24}$$

where $G_{m''} = g_{m''} e^{im''(-\varphi_k)}$ and we can do the same orthogonality on Eq. (3.22). Eq. (3.23) can be transformed into a big matrix which is given by

$$\begin{pmatrix} F_{11} & F_{12} \\ F_{21} & F_{22} \end{pmatrix} \begin{pmatrix} A \\ B \end{pmatrix} = \begin{pmatrix} G \\ G' \end{pmatrix} \tag{3.25}$$

where

$$F_{11} = \begin{pmatrix} e^{-iM\delta_1} f_{-M1} & \cdots & e^{-iM\delta_{2M+1}} f_{-M(2M+1)} \\ \vdots & \ddots & \vdots \\ e^{iM\delta_1} f_{M1} & \cdots & e^{iM\delta_{2M+1}} f_{M(2M+1)} \end{pmatrix}, \tag{3.26}$$

$$F_{12} = \begin{pmatrix} e^{-iM\delta_1} f'_{-M1} & \cdots & e^{-iM\delta_{2M+1}} f'_{-M(2M+1)} \\ \vdots & \ddots & \vdots \\ e^{iM\delta_{2M+1}} f'_{M1} & \cdots & e^{iM\delta_{2M+1}} f'_{M(2M+1)} \end{pmatrix}, \tag{3.27}$$

$$F_{21} = \begin{pmatrix} e^{-iM\delta_1} (\Re_1) f_{-M1} & \cdots & e^{-iM\delta_{2M+1}} (\Re_{2M+1}) f_{-M(2M+1)} \\ \vdots & \ddots & \vdots \\ e^{iM\delta_1} (\Re_1) f_{M1} & \cdots & e^{iM\delta_{2M+1}} (\Re_{2M+1}) f_{M(2M+1)} \end{pmatrix}, \tag{3.28}$$

and

$$F_{22} = \begin{pmatrix} e^{-iM\delta_1} (\Re'_1) f'_{-M1} & \cdots & e^{-iM\delta_{2M+1}} (\Re'_{2M+1}) f'_{-M(2M+1)} \\ \vdots & \ddots & \vdots \\ e^{iM\delta_{2M+1}} (\Re'_1) f'_{M1} & \cdots & e^{iM\delta_{2M+1}} (\Re'_{2M+1}) f'_{M(2M+1)} \end{pmatrix}. \tag{3.29}$$

The unknown matrix elements

$$A = \begin{pmatrix} a_{-M1} \\ \vdots \\ a_{M2M+1} \end{pmatrix} \tag{3.30}$$

and

$$B = \begin{pmatrix} b_{-M1} \\ \vdots \\ b_{M2M+1} \end{pmatrix} \tag{3.31}$$

can be solved in the numerical method for a given

$$G = \begin{pmatrix} G_{-M} \\ \vdots \\ G_M \end{pmatrix}$$

and

$$G' = \begin{pmatrix} (\Re_{inc})G_{-M} \\ \vdots \\ (\Re_{inc})G_M \end{pmatrix} .$$

Appendix gives the detailed derivation of the matrix in Dresselhaus-type SOI system. The numerical result of Eq. (3.30) and Eq. (3.31) can be used to obtain the total wave function Eq. (3.23) so that the spin density is determined. Also, we can observe the spin density pattern via the incident angle φ_k in the summation.

3.2 Linear-k Dresselhaus SOI

3.2.1 Coupled cylindrical wave representations

From the section 2.2, we know that the direction of the propagating of the incident plane wave along the $\hat{x}$ axis in linear-k Dresselhaus SOI system. Then, in cylindrical coordinate, incident plane wave has energy ε, momentum γ and helicity $\eta = +$, can be expansion of

partial waves

$$\psi_{in,+} = \sum_{m=-\infty}^{\infty} \frac{i^m}{2\sqrt{2}} \begin{pmatrix} \left[H_m^{(2)}(\gamma r) + H_m^{(1)}(\gamma r)\right] e^{im(\varphi)} \\ (i)\left[H_{m-1}^{(2)}(\gamma r) + H_{m-1}^{(1)}(\gamma r)\right] e^{i(m-1)(\varphi)} \end{pmatrix} . \tag{3.32}$$

and m is the total angular momentum which is conserved during the scattering. The energy eigenstate of the linear-k DSOI Hamiltonian can be written as

$$\psi_m = \begin{pmatrix} e^{im\varphi}\left[a_m H_m^{(1)}(\gamma r) + c_m H_m^{(1)}(\gamma' r) + \frac{i^m}{2\sqrt{2}} H_m^{(2)}(\gamma r)\right] \\ e^{i(m-1)\varphi}\left[i a_m H_{m-1}^{(1)}(\gamma r) - c_m i H_{m-1}^{(1)}(\gamma' r) + \frac{i^m}{2\sqrt{2}}(i) H_{m-1}^{(2)}(\gamma r)\right] \end{pmatrix} \tag{3.33}$$

where

$$\varepsilon = \gamma^2 + \beta_1 \kappa^2 \gamma = \gamma'^2 - \beta_1 \kappa^2 \gamma'.$$

The first and third terms have positive helicity while the second terms have the negative helicity. Here $H^{(1,2)}$ refers to the Hankel functions of the first and second kind respectively, and $H^{(1)}[H^{(2)}]$ is an outgoing (incoming) cylindrical wave. The most general eigenstates is a superposition of ψ_m, where the coefficients a_m and c_m are determined by boundary conditions. On the other hand, d_m is determined by the initial condition in Eq. (3.32), so we can obtain $d_m = \frac{i^m}{2\sqrt{2}}$. It means that the incident plane wave has $\eta = +$, then by comparing Eq. (3.33); the incoming wave (the second kind of the Hankel function) only has positive helicity, so d_m can be obtained. For a "hard " wall boundary (i.e. $\psi_m = 0 \; at \; r = R$), the coefficient can be given by

$$\begin{aligned} a_m &= -\frac{i^m}{2\sqrt{2}} \frac{H_m^{(1)}(\tilde{\gamma}') H_{m-1}^{(2)}(\tilde{\gamma}) + H_m^{(2)}(\tilde{\gamma}) H_{m-1}^{(1)}(\tilde{\gamma}')}{H_m^{(1)}(\tilde{\gamma}) H_{m-1}^{(1)}(\tilde{\gamma}') + H_m^{(1)}(\tilde{\gamma}') H_{m-1}^{(1)}(\tilde{\gamma})} \quad , \\ c_m &= \frac{i^m}{2\sqrt{2}} \frac{H_m^{(1)}(\tilde{\gamma}) H_{m-1}^{(2)}(\tilde{\gamma}) - H_m^{(2)}(\tilde{\gamma}) H_{m-1}^{(1)}(\tilde{\gamma})}{H_m^{(1)}(\tilde{\gamma}) H_{m-1}^{(1)}(\tilde{\gamma}') + H_m^{(1)}(\tilde{\gamma}') H_{m-1}^{(1)}(\tilde{\gamma})} \quad , \end{aligned} \tag{3.34}$$

where we define $\tilde{\gamma} \equiv \gamma R$ and $\tilde{\gamma}' \equiv \gamma' R$. The total wave function is the summation of partial wave can be represented by

$$\psi_{total} = \sum_m \psi_m \quad . \tag{3.35}$$

The Rashba scattering model has been investigated in [16].

To produce the recursion relation of the total wave function, we simplify Eq. (3.33)

$$\psi_m = \begin{pmatrix} e^{im\varphi} A_{+m} \\ e^{i(m-1)\varphi} B_{+m} \end{pmatrix} \tag{3.36}$$

where

$$\begin{aligned} A_{+m} &= a_m H_m^{(1)}(\gamma r) + c_m H_m^{(1)}(\gamma' r) + H_m^{(2)}(\gamma r) \\ B_{+m} &= i a_m H_{m-1}^{(1)}(\gamma r) - c_m i H_{m-1}^{(1)}(\gamma' r) + i H_{m-1}^{(2)}(\gamma r) \end{aligned} \quad . \tag{3.37}$$

We would obtain the relation of the coefficients

$$\begin{aligned} a_{-m+1} &= i^{-2m+1} a_m \\ c_{-m+1} &= -i^{-2m+1} c_m \end{aligned} \tag{3.38}$$

and

$$\begin{aligned} B_{+,-m+1} &= (-1)^m i A_{+,m} \\ B^*_{+,-m+1} &= -(-1)^m i A^*_{+,m} \quad . \end{aligned} \tag{3.39}$$

from the coefficient Eq. (3.34) if we have the properties of Hankel functions.

$$H_{-m}(z) = (-1)^m H_m(z) \tag{3.40}$$

The spin density of the total wave function in Eq. (3.32) for linear-k DSOI system can be obtained in analytical form if we use the recursion relation in Eq. (3.39). However,

the cubic-k DSOI system has to be solved in numerical method. The analytical form of the spin density is much more powerful which can be compared with the Rashba SOI scattering case [28].

3.3 Scattering of the scattering state

The scattering of the scattering state is composed of two kinds of outgoing waves (helicity $\eta = \pm$) which resulted from scattering upon a hard disk. We change the helicity of incident plane wave which is from the previous case and then the scattering process is analogical. But the quantity of spin density is slightly different.

3.4 Spin density of the scattering state

In the section we focus on the spin density of the scattering state both in linear-k DSOI and cubic-k DSOI systems. The spin density distribution is very important since we observe the polarization around the disk from the distribution. Moreover, for a given incident angle φ_k, we can obtain a spin density distribution. For the specific incident angle, it can be compared with the one in the Rashba SOI system. At the same time, it is important is to know the cubic-k contribution by comparing the in linear-k DSOI with cubic-k DSOI systems. And then from the energy dispersion in cubic-k DSOI systems which was derived in section 2.2, we know that the scattering process is the same due to the same energy dispersion when the incident angle φ_k is equal to $2n\pi$ (n is integer). In contrast, at the other incident angle, the cubic-k SOI contribution is considerable. Here we must use the numerical method to deal with the spin density in cubic-k DSOI system, but the spin density can be obtained analytically in linear-k DSOI system.

The spin density on linear-k DSOI can be evaluated lightly since the total wave function can be expressed in analytical form Eq. (3.33). By the definition, the spin density

$S_z(r,\varphi)$ in units of $\hbar/2$, is given by

$$S_z(r,\varphi) = \psi^{+}_{total}\sigma_z\psi_{total} \tag{3.41}$$

where σ_z is the Pauli matrix.

Substituting Eq. (3.33) into Eq. (3.41) the spin density becomes

$$\begin{aligned}
&S_z(r,\varphi)\\
&= \tfrac{1}{8}\sum_{m,m'} i^{m'-m}\begin{pmatrix} A^*_{+m}e^{-im\varphi} & B^*_{+m}e^{-i(m-1)\varphi}\end{pmatrix}\begin{pmatrix}1 & 0\\ 0 & -1\end{pmatrix}\begin{pmatrix} A_{+m'}e^{im'\varphi}\\ B_{+m'}e^{i(m'-1)\varphi}\end{pmatrix}\\
&= \tfrac{1}{8}\sum_{m,m'}\left[i^{m'-m}\cos\left((m'-m)\varphi\right) + i^{(m'-m+1)}\sin\left((m'-m)\varphi\right)\right]\left(A^*_{+m}A_{+m'} - B^*_{+m}B_{+m'}\right)
\end{aligned} \tag{3.42}$$

where the elements are described in Eq. (3.37) and Eq. (3.38) . The spin density whose φ dependence include odd function and even function (i.e. $\sin\left((m'-m)\varphi\right)$ *and* $\cos\left((m'-m)\varphi\right)$) . In addition, we reconsider recursion relation Eq. (3.39) which is useful to obtain the relation between the spin density $S_z(r,\varphi)$ and φ dependence.

$$\sum_{m,m'}\left[i^{m'-m}\cos\left((m'-m)\varphi\right)\right]F(r) = 0 \tag{3.43a}$$

$$\sum_{m,m'}\left[i^{(m'-m+1)}\sin\left((m'-m)\varphi\right)\right]F(r) = \sum_{m,m'} 2\sin\left((m'-m)\varphi\right)\left(A^*_{+m}A_{+m'}\right)i^{(m'-m+1)} \tag{3.43b}$$

where $F(r) = \left(A^*_{+m}A_{+m'} - B^*_{+m}B_{+m'}\right)$ is only radial dependent.

Therefore, we substitutes Eq. (3.43) into account that the spin density Eq. (3.42) can be obtained

$$S_z(r,\varphi) = \frac{1}{4}\sum_{m,m'}\sin\left((m'-m)\varphi\right)\left(A^*_{+m}A_{+m'}\right)i^{(m'-m+1)} \quad . \tag{3.44}$$

As a result, the $\varphi-$dependence in spin density exhibits odd parity from the analytical form Eq. (3.44) apparently (i.e. $S_z(r,-\varphi) = -S_z(r,\varphi)$). Hence, we conjecture that the spin density in the cubic-k DOS system would have a similar result but something is different due to the contribution from cubic-k term. The conjectural result in the cubic-k system about the spin density from the linear-k system is useful for us to estimate the result from the numerical method.

3.5 Particle continuity equation

In quantum mechanics, calculating current is crucial to applications. A widely accepted approach is using the correspondence regulation from classical to quantum mechanics. From the Schrödinger equation, we have $H\psi = i\frac{\partial}{\partial t}\psi$ and $(H\psi)^\dagger = -i\frac{\partial}{\partial t}\psi$. Notice here the transposition in the symbol $\dagger$ only acts on the spin index . We can use the above two equations to get the particle continuity equation.

$$\frac{\partial}{\partial t}\psi^\dagger\psi = \frac{1}{i}\left[\psi^\dagger\left(H\psi\right) - \left(H\psi\right)^\dagger\psi\right] \tag{3.45}$$

or

$$\frac{\partial}{\partial t}n = -\vec{\nabla}\cdot\vec{j} \tag{3.46}$$

where $n = \psi^\dagger\psi$ is the particle density and $\vec{j}$ is the particle current density.

It describes the conservation of the particle number. In the derivation below, we use the following Hamiltonian:

$$H = -\nabla^2 - \kappa^2\beta_1(k_x\sigma_x - k_y\sigma_y) + \beta_3(k_xk_y^2\sigma_x - k_yk_x^2\sigma_y) + V(\vec{r}) \tag{3.47}$$

In Eq. (3.45) the first term is the kinetic energy. The second and third terms are the Dresselhaus spin-orbit coupling, which has been extensively studied recently. Next we

substitute the Hamiltonian Eq. (3.47) into Eq. (3.45), and Eq. (3.45) becomes

$$\frac{\partial}{\partial t}\psi^\dagger\psi = \frac{1}{i}\left\{\begin{array}{l} -[\psi^\dagger\nabla^2\psi - (\nabla^2\psi^\dagger)\psi] - \kappa^2\beta_1[\psi^\dagger\sigma_x(k_x\psi) + (k_x\psi^\dagger)\sigma_x\psi] + \\ \kappa^2\beta_1[\psi^\dagger\sigma_y(k_y\psi) + (k_y\psi^\dagger)\sigma_y\psi] + \beta_3[\psi^\dagger\sigma_x(k_xk_y^2\psi) + (k_xk_y^2\psi^\dagger)\sigma_x\psi] \\ -\beta_3[\psi^\dagger\sigma_y(k_yk_x^2\psi) + (k_yk_x^2\psi^\dagger)\sigma_y\psi] \end{array}\right\} \tag{3.48}$$

And we have the

$\vec{k} = \frac{1}{i}\vec{\nabla} = \frac{1}{i}(\hat{x}\nabla_x + \hat{y}\nabla_y)$. After long careful calculations from Eq. (3.45) and Eq. (3.48), we obtain

$$\frac{\partial}{\partial t}n = -\vec{\nabla}\cdot(\vec{j}^{conv} + \vec{j}^{extra}) \tag{3.49}$$

where

$$\begin{aligned} \vec{j}^{conv} &= -i[\psi^\dagger(\vec{\nabla}\psi) + (\vec{\nabla}\psi^\dagger)\psi] \\ \vec{j}^{extra} &= \vec{j}^{L} + \vec{j}^{C} \\ \vec{j}^{L} &= -\kappa^2\beta_1[\psi^\dagger(\hat{x}\sigma_x - \hat{y}\sigma_y)\psi] \\ \vec{j}^{C} &= -[\beta_3\psi^\dagger(\hat{y}\sigma_x - \hat{x}\sigma_y)(\nabla_x\nabla_y\psi) + \beta_3(\nabla_x\nabla_y\psi^\dagger)(\hat{y}\sigma_x - \hat{x}\sigma_y)\psi] + [\beta_3(\nabla_i\psi^\dagger)(\hat{x}\sigma_x - \hat{y}\sigma_y)(\nabla_i\psi)] \\ &\qquad (i = x, y, z)\text{.....repeated index connection adopted} \end{aligned} \tag{3.50}$$

Appendix B gives the detailed calculation of the particle continuity equation in Dresselhaus SOI system.

Here $\vec{j}^{conv}$ is a " conventional term ". This term is general for any potential $V(\vec{r})$ in Hamiltonian if the potential is position dependent. And the main source to induce an extra term of the particle current $\vec{j}^{extra}$ comes from Dresselhaus spin orbit coupling which include linear term $\vec{j}^{L}$ and cubic term $\vec{j}^{C}$.

In Rashba SOI system in Eq. (3.51), we get the same result in Eq. (3.52) except for

the extra term in Eq. (3.53).

$$H_R = -\nabla^2 + \alpha(k_x\sigma_y - k_y\sigma_x) + V(\vec{r}) \tag{3.51}$$

$$\vec{j} = \vec{j}^{conv} + \vec{j}^{extra} \tag{3.52}$$

where

$$\vec{j}^{extra} = \vec{j}^{R} = \alpha\psi^\dagger(\vec{\sigma} \times \hat{z})\psi \tag{3.53}$$

However, we discuss the particle current in some complex system with SOI such as Dresselhaus SOI in Eq. (3.47) and Rashba SOI in Eq. (3.51) in which the momentum appears in the "potential " of the Hamiltonian of semiconductors that the extra term must exit. In our case, the number of particle must conserve during the scattering process without any bias or EM fields.

Chapter 4

Numerical results and discussions

4.1 Results for linear-k Dresselhaus SOI

We has studied the results of the scattering in linear-k Dresselhaus system. In chapter 3, the spin density of the total wave function would be solved in numerical method as we do in this chapter just like solving the Rashba scattering problem [28]. But we find the recursion relation of the coefficients of the wave function which can be used to simplify the spin density toughly so that we have the analytical form. However, we can compare the numerical results with the analytical results. The plane wave incident a hard wall disk in linear-k Dresselhaus system with the helicity $\eta = +$, the incident energy ε=7.7 (in unit of ε^*), and the incident angle φ_k=0 (the energy unit $\varepsilon^* = 8.977$ meV).The spin density of the total function has the analytical form

$$S_z(r,\varphi) = \psi^+_{total}\sigma_z\psi_{total} = \frac{1}{4}\sum_{m,m'} \sin\left((m'-m)\varphi\right)\left(A^*_{+m}A_{+m'}\right) i^{(m'-m+1)} \tag{4.1}$$

where

$$A_{+m} = a_m H^{(1)}_m(\gamma r) + c_m H^{(1)}_m(\gamma' r) + H^{(2)}_m(\gamma r) \tag{4.2}$$

whose coefficients are

$$a_m = -\frac{H_m^{(1)}(\tilde{\gamma}')H_{m-1}^{(2)}(\tilde{\gamma}) + H_m^{(2)}(\tilde{\gamma})H_{m-1}^{(1)}(\tilde{\gamma}')}{H_m^{(1)}(\tilde{\gamma})H_{m-1}^{(1)}(\tilde{\gamma}') + H_m^{(1)}(\tilde{\gamma}')H_{m-1}^{(1)}(\tilde{\gamma})} \tag{4.3}$$

and

$$c_m = \frac{H_m^{(1)}(\tilde{\gamma})H_{m-1}^{(2)}(\tilde{\gamma}) - H_m^{(2)}(\tilde{\gamma})H_{m-1}^{(1)}(\tilde{\gamma})}{H_m^{(1)}(\tilde{\gamma})H_{m-1}^{(1)}(\tilde{\gamma}') + H_m^{(1)}(\tilde{\gamma}')H_{m-1}^{(1)}(\tilde{\gamma})} \quad . \tag{4.4}$$

The numerical results of the spin density from 3.2.1 we can solve the boundary condition by using numerical method. And then the distribution of the spin density and the probability density of the total wave function are obtained in Fig. 4.1 and Fig. 4.2 respectively.

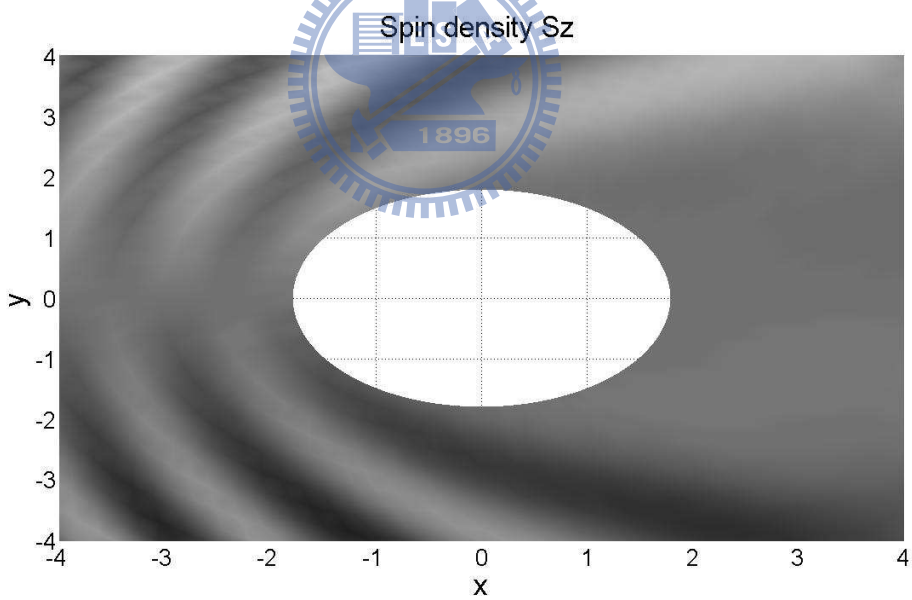

Figure 4.1: Distribution of the out-of-plane spin density S_z. The plane wave incident a hard wall disk in linear-k Dresselhaus system with the helicity $\eta = +$, the incident energy ε=7.7, and the incident angle φ_k=0. Lighter regions means the region whose spin density S_z >0 (spin up). And the darker regions represent the region of spin down .

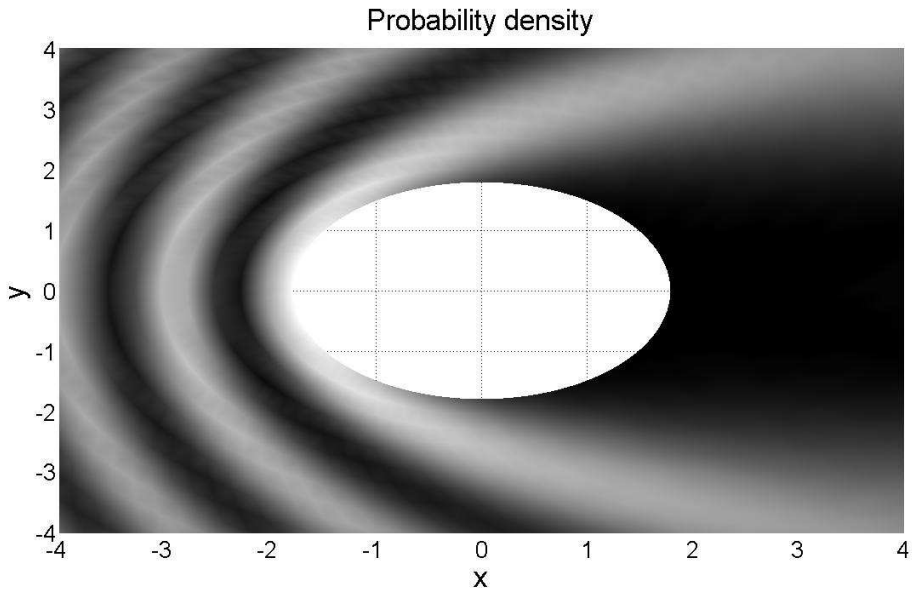

Figure 4.2: The spatial dependence of the magnitude of the total wave function probability density. Out of the white circle is the region with finite Dresselhaus SOI. Apparently, when the plane wave propagates along the x axis, the probability density is almost zero behind the disk due to the hard wall disk .

The spin density function is the odd function of φ from Eq. (4.1), i.e. $S_z(r, -\varphi) = -S_z(r, \varphi)$. The property from the analytical result is consistent with the distribution of the spin density pattern plotted in Fig. 4.1. Also, Fig. 4.2 show that the total wave function density is almost zero behind the disk due to the hard wall disk.

For a larger incident energy ε=13.23 (in unit of ε^*) , we obtain the spin density plotted in Fig. 4.3. The total wave function probability density is plotted in Fig. 4.4, where other parameters of the incident plane wave and the linear-k DSOI constant are fixed. From Fig. 4.3 and Fig. 4.2, we can conclude that the concentration of spin density (fringes) become higher by larger incident energy. The energy dispersion of the incident wave with helicity η which we derived in chapter 1 shows that the momentum is independent of the incident angle φ_k and then the effective magnetic filed is perpendicular to momentum in linear-k Dresselhaus system. Hence, the distribution of the probability density and spin density in linear-k Dresselhaus system are just rotated by the incident wave angle but the patterns are the same.

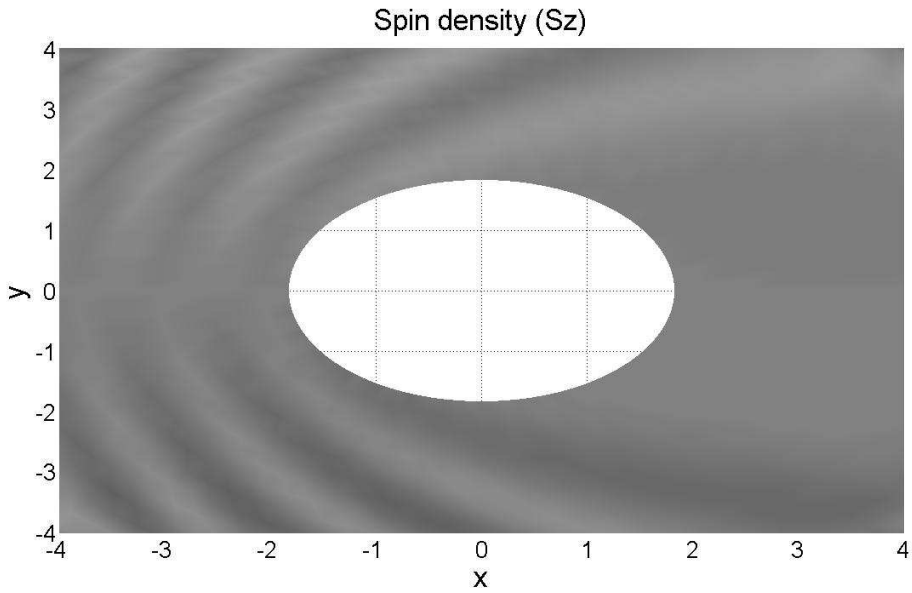

Figure 4.3: Distribution of the out-of-plane spin density S_z. The plane wave incident a hard wall disk in linear-k Dresselhaus system with the helicity $\eta = +$, the incident energy ε=13.23, and the incident angle φ_k=0. Lighter regions means the region whose spin density S_z >0 (spin up) . And the darker regions represent the region of spin down .

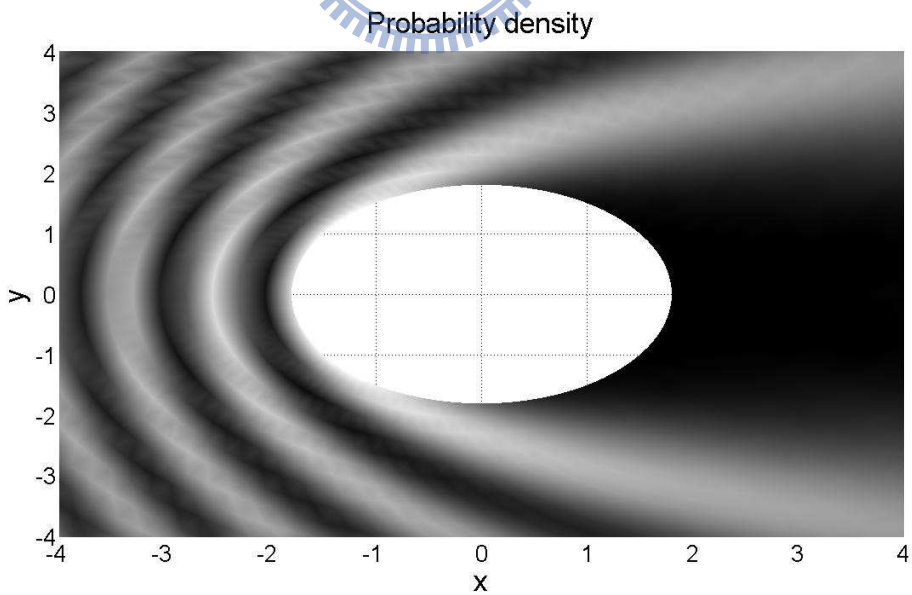

Figure 4.4: The spatial dependence of the magnitude of the total wave function probability density. Out of the white circle is the region with finite Dresselhaus SOI. Apparently, when the plane wave propagates along the x axis, the probability density is almost zero behind the disk due to the hard wall disk.

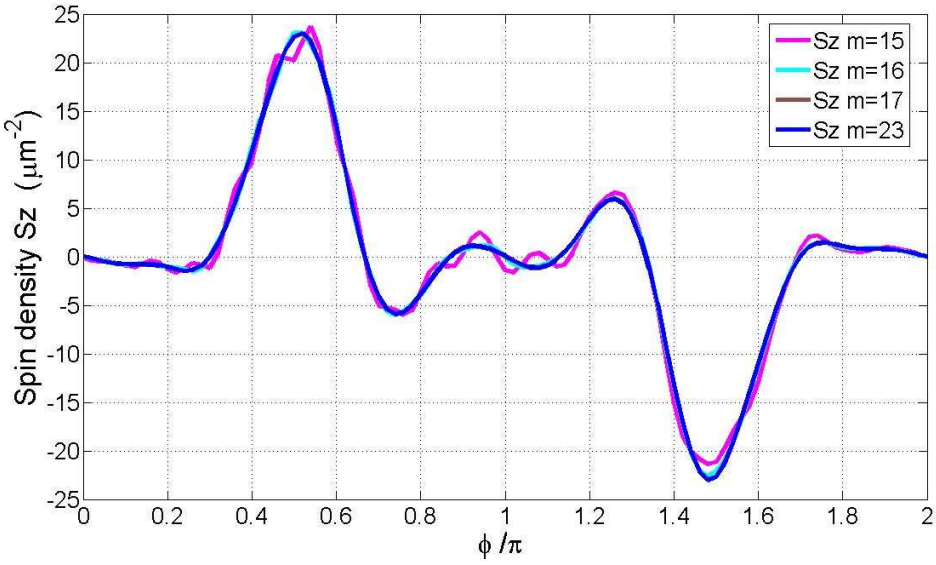

Figure 4.5: The quality the spin density S_z determining the number m as function of φ for a central hard wall disk where m represents the number of the partial waves we must sum. Apparently, the line of the spin density corresponding to the distribution of the spin density Fig. 4.1 at r=2 is saturated for a larger m. And the probability density also has the same situation.

4.2 Results for cubic-k Dresselhaus SOI and more Discussions

In the case of cubic-k Dresselhaus, we must deal with a troublesome numerical problem. However, it doesn't saturate or converge to a value. Here we replace the plane wave with the cylindrical wave to check the sliced method in *appendix C*. We consider a cylindrical wave incidents a Dresselhaus SOI disk and we both use the sliced and non-sliced methods. And then we make a comparison between analytical results and numerical approach in cylindrical wave case in order to check our numerical method. Results in *appendix C* show that the numerical method is feasible for cylindrical wave in Dresselhaus SOI case.

4.3 Discussion on the connection of spin density with the plane wave direction

We make a discussion on the connection of spin density with the plane wave direction in Dresselhaus SOI system.

The energy dispersion in the linear-k Dresselhaus system we derived in Chapter 2

$$\varepsilon = k^2 \pm \beta\kappa^2 k \tag{4.5}$$

and the spin density Eq. (4.1) we driven in Chapter 3 which can be evaluated easily. For a given incident plane wave with energy ε, helicity η, and incident angle φ_k, we can obtain the momentum k by solving Eq. (4.5) so that the corresponding momentum is independent of incident angle φ_k. Also, we know that the effective magnetic field is always perpendicular to the momentum. Hence, we can surmise that the spin density and probability density patterns are just rotated an angle for a different incident angle φ_k in linear-k Dresselhaus system and the distribution and the strength of them are analogical.

In the cubic-k Dresselhaus system the energy dispersion we driven

$$\varepsilon = k^2 \pm \beta_1 k\sqrt{\kappa^4 + [\frac{\beta_3}{2\beta_1}k^2\sin(2\varphi_k)]^2 - \frac{\beta_3}{\beta_1}k^2\kappa^2\sin^2(2\varphi_k)} \tag{4.6}$$

and then we can obtain the momentum from Eq. (4.6). Obviously, the momentum is dependent of φ_k so that we can adjust that both the spin density and probability density patterns in cubic-k Dresselhaus system are dependent of φ_k. The scattering process in cubic-k Dresselhaus system with a different incident angle φ_k is more complex than in linear-k Dresselhaus system.

Chapter 5

Future work

In the future, we continue to accomplish the cubic-k Dresselhaus scattering problem. The scattering of incoming spin-polarized beam of electrons in DSOI system could provide a way for detecting spin-current and then serves as a basis considering a magnetic flux in the disk. Also, such a setting of SOI can be used to produce a source of spin-polarized electrons, which has a variety of potential applications in spintronics processing.

Appendix A

Simplify the boundary condition problem

The total wave function in Dresselhaus system can be written as

$$\psi_{total}(R,\varphi,\varphi_k)$$

$$= \begin{pmatrix} \sum_{m=-M}^{M}\left(\sum_{n=1}^{2M+1}\Delta\delta e^{im(\varphi+\delta_n)}[a_{mn}f_{mn}+b_{mn}f'_{mn}]+g_m e^{im(\varphi-\varphi_k)}\right) \\ \sum_{m'=-M}^{M}\left(\sum_{n=1}^{2M+1}\Delta\delta e^{im'(\varphi+\delta_n)}[a_{m'n}(\Re_n)f_{m'n}+b_{m'n}(\Re'_n)f'_{m'n}]+(\Re_{inc})g_{m'}e^{im'(\varphi-\varphi_k)}\right) \end{pmatrix}$$

$$= 0 \tag{A.1}$$

where $f_{mn} = H_m^{(1)}(\gamma_n R)$, $f'_{mn} = H_m^{(1)}(\gamma'_n R)$, $g_m = \frac{i^m}{2\sqrt{2}}H_m^{(2)}(\gamma R)$, and

$$N = 2M+1 \ , \Delta\delta = \frac{2\pi}{2M+1}, \delta_n = n\Delta\delta = n\frac{2\pi}{2M+1} \quad .$$

Besides, in Eq. (A.1) the values of ratio we driven in Chapter 2 are

$$(\Re_{inc}) = -e^{i(\varphi_k)}\sqrt{\frac{\kappa^2 e^{-i(2\varphi_k)} + \frac{\beta_3}{2\beta_1} ik^2 \sin(2\varphi_k)}{\kappa^2 e^{i(2\varphi_k)} - \frac{\beta_3}{2\beta_1} ik^2 \sin(2\varphi_k)}} \tag{A.2a}$$

$$(\Re_n) = e^{-i\delta_n}\sqrt{-\frac{(i\kappa^2 e^{i2\delta_n} + \frac{\beta_3}{\beta_1}\frac{\gamma_n^2}{2}\sin(2\delta_n))}{(i\kappa^2 e^{-i2\delta_n} - \frac{\beta_3}{\beta_1}\frac{\gamma_n^2}{2}\sin(2\delta_n))}} \tag{A.2b}$$

$$(\Re'_n) = -e^{-i\delta_n}\sqrt{-\frac{(i\kappa^2 e^{i2\delta_n} + \frac{\beta_3}{\beta_1}\frac{(\gamma'_n)^2}{2}\sin(2\delta_n))}{(i\kappa^2 e^{-i2\delta_n} - \frac{\beta_3}{\beta_1}\frac{(\gamma'_n)^2}{2}\sin(2\delta_n))}}\ . \tag{A.2c}$$

Here we use the orthogonal property of φ so that we integrals over φ in Eq. (A.1) where the φ ranges from 0 to 2π and the the number m'' ranges $-M$ to M.
(i.e. $\frac{1}{2\pi}\int_0^{2\pi} d\varphi e^{-im''\varphi}$.)
The first low of Eq. (A.1) after integrating can written as

$$\sum_{m=-M}^{M}\left(\sum_{n=1}^{2M+1}\frac{1}{2\pi}\int_0^{2\pi} d\varphi e^{-im''\varphi} e^{im(\varphi+\delta_n)}\Delta\delta[f_{mn}a_{mn} + f'_{mn}b_{mn}] + \frac{1}{2\pi}\int_0^{2\pi} d\varphi e^{-im''\varphi} g_m e^{im(\varphi-\varphi_k)}\right) = 0 \tag{A.3}$$

$$\sum_{m=-M}^{M}\left(\sum_{n=1}^{2M+1} e^{im\delta_n}\Delta\delta[f_{mn}a_{mn} + f'_{mn}b_n]\tfrac{1}{2\pi}\int_0^{2\pi} d\varphi e^{i(m-m'')\varphi} + g_m e^{im(-\varphi_k)}\tfrac{1}{2\pi}\int_0^{2\pi} d\varphi e^{i(m-m'')\varphi}\right) = 0$$

$$\sum_{m=-M}^{M}\left(\sum_{n=1}^{2M+1} e^{im\delta_n}\Delta\delta[f_{mn}a_{mn} + f'_{mn}b_{mn}]\delta_{mm''} + g_m e^{im(-\varphi_k)}\delta_{mm''}\right) = 0$$

($\delta_{mm''}$ is delta function [30])

$$\sum_{n=1}^{2M+1}\left(e^{im''\delta_n}\Delta\delta[f_{m''n}a_{m''n} + f'_{m''n}b_{m''n}]\right) + g_{m''}e^{im''(-\varphi_k)}) = 0$$

After calculation, we obtain

$$\sum_{n=1}^{2M+1}\left(e^{im''\delta_n}[f_{m''n}a_{m''n}+f'_{m''n}b_{m''n}]\right)=-\frac{1}{\Delta\delta}g_{m''}e^{im''(-\varphi_k)} \quad . \tag{A.4}$$

In the same way, we deal with the second low of Eq. (A.1).

$$\sum_{m'=-M}^{M}\left(\begin{array}{l}\sum_{n=1}^{2M+1}\frac{1}{2\pi}\int_0^{2\pi}d\varphi e^{-im''\varphi}e^{im'(\varphi+\delta_n)}\Delta\delta[(\Re_n)f_{m'n}a_{m'n}+(\Re'_n)f'_{m'n}b_{m'n}]\\ +\frac{1}{2\pi}\int_0^{2\pi}d\varphi e^{-im''\varphi}e^{i\theta_{inc}}g_{m'}e^{im'(\varphi-\varphi_k)}\end{array}\right)=0 \tag{A.5}$$

$$\sum_{m'=-M}^{M}\left(\begin{array}{l}\sum_{n=1}^{2M+1}e^{im'\delta_n}\Delta\delta[(\Re_n)f_{m'n}a_n+(\Re'_n)f'_{m'n}b_n]\frac{1}{2\pi}\int_0^{2\pi}d\varphi e^{i(m'-m'')\varphi}\\ +(\Re_{inc})g_{m'}e^{im'(-\varphi_k)}\frac{1}{2\pi}\int_0^{2\pi}d\varphi e^{i(m'-m'')\varphi}\end{array}\right)=0$$

$$\sum_{m'=-M}^{M}\left(\sum_{n=1}^{2M+1}e^{im'\delta_n}\Delta\delta[(\Re_n)f_{m'n}a_n+(\Re'_n)f'_{m'n}b_n]\delta_{m'm''}+(\Re_{inc})g_{m'}e^{im'(-\varphi_k)}\delta_{m'm''}\right)=0$$

$$\sum_{n=1}^{2M+1}\left(e^{im''\delta_n}\Delta\delta[(\Re_n)f_{m''n}a_n+(\Re'_n)f'_{m''n}b_n]+(\Re_{inc})g_{m''}e^{im''(-\varphi_k)}\right)=0$$

Therefore, we also obtain the simplified form which is similar with Eq. (A.4).

$$\sum_{n=1}^{2M+1}e^{im''\delta_n}[(\Re_n)f_{m''n}a_n+(\Re'_n)f'_{m''n}b_n]=-\frac{1}{\Delta\delta}(+\Re_{inc})g_{m''}e^{im''(-\varphi_k)} \tag{A.6}$$

We consider the number m'' which ranges from $-M$ to M and then we can use Eq. (A.4) and Eq. (A.6) to demonstrate a big matrix.

$$\begin{pmatrix}F_{11} & F_{12}\\ F_{21} & F_{22}\end{pmatrix}\begin{pmatrix}A\\ B\end{pmatrix}=\begin{pmatrix}G\\ G'\end{pmatrix} \tag{A.7}$$

Each element of Eq. (A.7) are given respectively as following :

$$F_{11} = \begin{pmatrix} e^{-iM\delta_1} f_{-M1} & \cdots & e^{-iM\delta_{2M+1}} f_{-M(2M+1)} \\ \vdots & \ddots & \vdots \\ e^{iM\delta_1} f_{M1} & \cdots & e^{iM\delta_{2M+1}} f_{M(2M+1)} \end{pmatrix} \tag{A.8a}$$

$$F_{12} = \begin{pmatrix} e^{-iM\delta_1} f'_{-M1} & \cdots & e^{-iM\delta_{2M+1}} f'_{-M(2M+1)} \\ \vdots & \ddots & \vdots \\ e^{iM\delta_{2M+1}} f'_{M1} & \cdots & e^{iM\delta_{2M+1}} f'_{M(2M+1)} \end{pmatrix} \tag{A.8b}$$

$$F_{21} = \begin{pmatrix} e^{-iM\delta_1} (\Re_1) f_{-M1} & \cdots & e^{-iM\delta_{2M+1}} (\Re_{2M+1}) f_{-M(2M+1)} \\ \vdots & \ddots & \vdots \\ e^{iM\delta_1} (\Re_1) f_{M1} & \cdots & e^{iM\delta_{2M+1}} (\Re_{2M+1}) f_{M(2M+1)} \end{pmatrix} \tag{A.8c}$$

$$F_{22} = \begin{pmatrix} e^{-iM\delta_1} (\Re'_1) f'_{-M1} & \cdots & e^{-iM\delta_{2M+1}} (\Re'_{2M+1}) f'_{-M(2M+1)} \\ \vdots & \ddots & \vdots \\ e^{iM\delta_{2M+1}} (\Re'_1) f'_{M1} & \cdots & e^{iM\delta_{2M+1}} (\Re'_{2M+1}) f'_{M(2M+1)} \end{pmatrix} \tag{A.8d}$$

$$A = \begin{pmatrix} a_{-M1} \\ \vdots \\ a_{M2M+1} \end{pmatrix} \quad , \quad B = \begin{pmatrix} b_{-M1} \\ \vdots \\ b_{M2M+1} \end{pmatrix} \tag{A.8e}$$

$$G = \begin{pmatrix} G_{-M} \\ \vdots \\ G_M \end{pmatrix} \quad , \quad G' = \begin{pmatrix} (\Re_{inc}) G_{-M} \\ \vdots \\ (\Re_{inc}) G_M \end{pmatrix} . \tag{A.8f}$$

We obtain the unknown coefficients of Eq. (A.8) by using numerical method to solve the matrix Eq. (A.7). Hence, the numerical result can be used to obtain the total wave function Eq. (A.1) so that the spin density is determined.

Appendix B

Derivation of spin density of the total wave function after scattering

The incident plane wave with helicity η and incident angle φ_k is

$$\psi_{in,\eta} = \frac{1}{\sqrt{2}} \begin{pmatrix} 1 \\ R \end{pmatrix} e^{ikr\cos(\varphi-\varphi_k)} = \frac{1}{\sqrt{2}} \begin{pmatrix} 1 \\ \eta R_{in} \end{pmatrix} e^{ikr\cos(\varphi-\varphi_k)} \tag{B.1}$$

$$= \frac{1}{2\sqrt{2}} \sum_{m=-\infty}^{\infty} \begin{pmatrix} i^m \left[H_m^{(2)}(kr) + H_m^{(1)}(kr)\right] e^{im(\varphi-\varphi_k)} \\ (\eta R_{in}) i^{m-1} \left[H_{m-1}^{(2)}(kr) + H_{m-1}^{(1)}(kr)\right] e^{i(m-1)(\varphi-\varphi_k)} \end{pmatrix} \tag{B.2}$$

$$= \frac{1}{2\sqrt{2}} \sum_{m=-\infty}^{\infty} i^m \begin{pmatrix} \left[H_m^{(2)}(kr) + H_m^{(1)}(kr)\right] e^{im(\varphi-\varphi_k)} \\ (-i\eta R_{in}) \left[H_{m-1}^{(2)}(kr) + H_{m-1}^{(1)}(kr)\right] e^{i(m-1)(\varphi-\varphi_k)} \end{pmatrix} . \tag{B.3}$$

For a given helicity $\eta = +$ and $\varphi_k = 0$ (propagate along x axis), the incident wave can be written as following

$$\psi_{in,+} = \frac{1}{2\sqrt{2}} \sum_{m=-\infty}^{\infty} i^m \begin{pmatrix} \left[H_m^{(2)}(kr) + H_m^{(1)}(kr)\right] e^{im(\varphi)} \\ (i) \left[H_{m-1}^{(2)}(kr) + H_{m-1}^{(1)}(kr)\right] e^{i(m-1)(\varphi)} \end{pmatrix} . \tag{B.4}$$

The energy eigenstates of the Schrodinger equation with energy ε and the angular momentum $(m+1/2)\hbar$ can be written as :

$$\psi_{+m} = \begin{pmatrix} e^{im\varphi}\left[a_m H_m^{(1)}(\gamma r) + c_m H_m^{(1)}(\gamma' r) + H_m^{(2)}(\gamma r)\right] \\ \\ e^{i(m-1)\varphi}\left[i a_m H_{m-1}^{(1)}(\gamma r) - c_m i H_{m-1}^{(1)}(\gamma' r) + (i) H_{m-1}^{(2)}(\gamma r)\right] \end{pmatrix} = \begin{pmatrix} e^{im\varphi} A_{+m} \\ e^{i(m-1)\varphi} B_{+m} \end{pmatrix} \tag{B.5}$$

where

$$A_{+m} = a_m H_m^{(1)}(\gamma r) + c_m H_m^{(1)}(\gamma' r) + H_m^{(2)}(\gamma r) \tag{B.6a}$$

$$B_{+m} = i a_m H_{m-1}^{(1)}(\gamma r) - c_m i H_{m-1}^{(1)}(\gamma' r) + (i) H_{m-1}^{(2)}(\gamma r) \tag{B.6b}$$

and

$$\varepsilon = \hbar^2\gamma^2/2m + \beta\gamma = \hbar^2\gamma'^2/2m - \beta\gamma' \quad . \tag{B.7}$$

Eq. (B.5) means that the total wave function ψ_{+m} has the incident wave which is propagating along x axis with incident energy ε, momentum γ, angular momentum $(m+1/2)\hbar$, and helicity $+$.

The most general eigenstate of the eigenequation is a superposition of the ψ_{+m}

$$\psi^{total} = \sum_m \psi_m^{total} = \frac{1}{2\sqrt{2}} \sum_m i^m \begin{pmatrix} A_{+m} e^{im\varphi} \\ B_{+m} e^{i(m-1)\varphi} \end{pmatrix} \tag{B.8}$$

, where a_m and c_m are determined by boundary condition.

For a hard disk

$$\psi_{total}(r = R) = 0 \ , \tag{B.9}$$

it can be shown that

$$a_m = -\frac{H_m^{(1)}(\tilde{\gamma}')H_{m-1}^{(2)}(\tilde{\gamma}) + H_m^{(2)}(\tilde{\gamma})H_{m-1}^{(1)}(\tilde{\gamma}')}{H_m^{(1)}(\tilde{\gamma})H_{m-1}^{(1)}(\tilde{\gamma}') + H_m^{(1)}(\tilde{\gamma}')H_{m-1}^{(1)}(\tilde{\gamma})} \tag{B.10a}$$

$$c_m = \frac{H_m^{(1)}(\tilde{\gamma})H_{m-1}^{(2)}(\tilde{\gamma}) - H_m^{(2)}(\tilde{\gamma})H_{m-1}^{(1)}(\tilde{\gamma})}{H_m^{(1)}(\tilde{\gamma})H_{m-1}^{(1)}(\tilde{\gamma}') + H_m^{(1)}(\tilde{\gamma}')H_{m-1}^{(1)}(\tilde{\gamma})} \tag{B.10b}$$

where $\tilde{\gamma} \equiv \gamma R$ and $\tilde{\gamma}' \equiv \gamma' R$.

The recursion relation of the Hankel function is

$$H_{-d}^{(1)2}(z) = (-1)^d H_d^{(1)2}(z) \tag{B.11}$$

We can find a ration in Eq. (B.10) through Eq. (B.11).

$$\begin{aligned} a_{-m+1} &= -\frac{H_{-m+1}^{(1)}(\tilde{\gamma}')H_{-m}^{(2)}(\tilde{\gamma})+H_{-m+1}^{(2)}(\tilde{\gamma})H_{-m}^{(1)}(\tilde{\gamma}')}{H_{-m+1}^{(1)}(\tilde{\gamma})H_{-m}^{(1)}(\tilde{\gamma}')+H_{-m+1}^{(1)}(\tilde{\gamma}')H_{-m}^{(1)}(\tilde{\gamma})} \\ &= -\frac{H_{m-1}^{(1)}(\tilde{\gamma}')H_m^{(2)}(\tilde{\gamma})+H_{m-1}^{(2)}(\tilde{\gamma})H_m^{(1)}(\tilde{\gamma}')}{H_{m-1}^{(1)}(\tilde{\gamma})H_m^{(1)}(\tilde{\gamma}')+H_{m-1}^{(1)}(\tilde{\gamma}')H_m^{(1)}(\tilde{\gamma})} \\ &= a_m \end{aligned} \tag{B.12}$$

$$\begin{aligned} c_{-m+1} &= \frac{H_{-m+1}^{(1)}(\tilde{\gamma})H_{-m}^{(2)}(\tilde{\gamma})-H_{-m+1}^{(2)}(\tilde{\gamma})H_{-m}^{(1)}(\tilde{\gamma})}{H_{-m+1}^{(1)}(\tilde{\gamma})H_{-m}^{(1)}(\tilde{\gamma}')+H_{-m+1}^{(1)}(\tilde{\gamma}')H_{-m}^{(1)}(\tilde{\gamma})} \\ &= \frac{H_{m-1}^{(1)}(\tilde{\gamma})H_m^{(2)}(\tilde{\gamma})-H_{m-1}^{(2)}(\tilde{\gamma})H_m^{(1)}(\tilde{\gamma})}{H_{m-1}^{(1)}(\tilde{\gamma})H_m^{(1)}(\tilde{\gamma}')+H_{m-1}^{(1)}(\tilde{\gamma}')H_m^{(1)}(\tilde{\gamma})} \\ &= -c_m \end{aligned} \tag{B.13}$$

Hence, we obtain recursion relations both of a_m and c_m

$$a_{-m+1} = a_m \tag{B.14a}$$

$$c_{-m+1} = -c_m \tag{B.14b}$$

which are useful. We take Eq. (B.14) into Eq. (B.6), and then obtain

$$\begin{aligned} B_{+,-m+1} &= a_{-m+1} i H^{(1)}_{-m}(\gamma r) - c_{-m+1} i H^{(1)}_{-m}(\gamma' r) + i H^{(2)}_{-m}(\gamma r) \\ &= a_m i(-1)^m H^{(1)}_m(\gamma r) + c_m i(-1)^m H^{(1)}_m(\gamma' r) + (-1)^m i H^{(2)}_m(\gamma r) \\ &= (-1)^m i \left[a_m H^{(1)}_m(\gamma r) + c_m H^{(1)}_m(\gamma' r) + H^{(2)}_m(\gamma r) \right] \\ &= (-1)^m i A_{+,m} \end{aligned} \tag{B.15}$$

$$B_{+,-m+1} = (-1)^m i A_{+,m} \tag{B.16a}$$

$$B^*_{+,-m+1} = -(-1)^m i A^*_{+,m} \tag{B.16b}$$

Therefore, $A_{+,m}$ can be replaced with $B_{+,-m+1}$ so that the spin density of the total wave function is

$$\begin{aligned} \langle S_z \rangle = \psi^+_{total} \sigma_z \psi_{total} &= \tfrac{1}{8} \sum_{m,m'} i^{m'-m} \begin{pmatrix} A^*_{+m} e^{-im\varphi} & B^*_{+m} e^{-i(m-1)\varphi} \end{pmatrix} \begin{pmatrix} 1 & 0 \\ 0 & -1 \end{pmatrix} \begin{pmatrix} A_{+m'} e^{im'\varphi} \\ B_{+m'} e^{i(m'-1)\varphi} \end{pmatrix} \\ &= \tfrac{1}{8} \sum_{m,m'} i^{m'-m} \begin{pmatrix} A^*_{+m} e^{-im\varphi} & B^*_{+m} e^{-i(m-1)\varphi} \end{pmatrix} \begin{pmatrix} A_{+m'} e^{im'\varphi} \\ -B_{+m'} e^{i(m'-1)\varphi} \end{pmatrix} \\ &= \tfrac{1}{8} \sum_{m,m'} i^{m'-m} \left(A^*_{+m} A_{+m'} e^{-im\varphi} e^{im'\varphi} - B^*_{+m} e^{-i(m-1)\varphi} B_{+m'} e^{i(m'-1)\varphi} \right) \\ &= \tfrac{1}{8} \sum_{m,m'} i^{m'-m} e^{i(m'-m)\varphi} \left(A^*_{+m} A_{+m'} - B^*_{+m} B_{+m'} \right) \\ &= \tfrac{1}{8} \sum_{m,m'} \left[i^{m'-m} \cos\left((m'-m)\varphi\right) + i^{(m'-m+1)} \sin\left((m'-m)\varphi\right) \right] \left(A^*_{+m} A_{+m'} - B^*_{+m} B_{+m'} \right) \end{aligned} \tag{B.17}$$

Apparently , the spin density of the total wave function Eq. (B.17) can be decomposed as a superposotion of the even function of φ and the odd function of φ .
(i.e.$\cos\left((m'-m)\varphi\right)$ and $\sin\left((m'-m)\varphi\right)$.)

The even function of φ part of Eq. (B.17) can be simplified by Eq. (B.16).

$$
\begin{aligned}
&\sum_{m,m'} \left[i^{m'-m}\cos\left((m'-m)\varphi\right)\right]\left(A^*_{+m}A_{+m'} - B^*_{+m}B_{+m'}\right) \\
&= \sum_{m,m'} \left[i^{m'-m}\cos\left((m'-m)\varphi\right)\right]\left(A^*_{+m}A_{+m'}\right) - \sum_{m,m'} \left[i^{m'-m}\cos\left((m'-m)\varphi\right)\right]\left(B^*_{+m}B_{+m'}\right) \\
&= \sum_{m,m'} \left[i^{m'-m}\cos\left((m'-m)\varphi\right)\right]\left(A^*_{+m}A_{+m'}\right) \\
&\quad - \sum_{m,m'} \left[i^{(-m'+1+m-1)}\cos\left((-m'+1+m-1)\varphi\right)\right]\left(B^*_{+,-m+1}B_{+,-m'+1}\right) \\
&= \sum_{m,m'} \cos\left((m'-m)\varphi\right)\left(A^*_{+m}A_{+m'}\right)\left[i^{m'-m} - i^{-(m'-m)}(-1)^{m'+m}\right] \\
&= 0
\end{aligned}
$$

Also, the odd function of φ part of Eq. (B.17) by Eq. (B.16).

$$
\begin{aligned}
&\sum_{m,m'} \left[i^{(m'-m+1)}\sin\left((m'-m)\varphi\right)\right]\left(A^*_{+m}A_{+m'} - B^*_{+m}B_{+m'}\right) \\
&= \sum_{m,m'} \left[i^{(m'-m+1)}\sin\left((m'-m)\varphi\right)\right]\left(A^*_{+m}A_{+m'}\right) - \sum_{m,m'} \left[i^{(m'-m+1)}\sin\left((m'-m)\varphi\right)\right]\left(B^*_{+m}B_{+m'}\right) \\
&= \sum_{m,m'} \left[i^{(m'-m+1)}\sin\left((m'-m)\varphi\right)\right]\left(A^*_{+m}A_{+m'}\right) \\
&\quad - \sum_{m,m'} \left[i^{(-m'+1+m-1+1)}\sin\left((-m'+1+m-1)\varphi\right)\right]\left(B^*_{+,-m+1}B_{+,-m'+1}\right) \\
&= \sum_{m,m'} \left[i^{(m'-m+1)}\sin\left((m'-m)\varphi\right)\right]\left(A^*_{+m}A_{+m'}\right) \\
&\quad + i^2 \sum_{m,m'} \left[i^{-(m'-m+1)}\sin\left((m'-m)\varphi\right)\right]\left(-(-1)^m i A^*_{+m} i(-1)^{m'} A_{+,m'}\right) \\
&= \sum_{m,m'} \sin\left((m'-m)\varphi\right)\left(A^*_{+m}A_{+m'}\right) i^{(m'-m+1)}\left[1 - i^{-2(m'-m+1)}(-1)^{m+m'}\right] \\
&= \sum_{m,m'} \sin\left((m'-m)\varphi\right)\left(A^*_{+m}A_{+m'}\right) i^{(m'-m+1)} 2
\end{aligned}
$$

Finally, the spin density of the total wave function can be obtained as

$$
\begin{aligned}
\langle S_z \rangle &= \psi^+_{total}\sigma_z\psi_{total} \\
&= \tfrac{1}{8}\sum_{m,m'} \sin\left((m'-m)\varphi\right)\left(A^*_{+m}A_{+m'}\right) i^{(m'-m+1)} 2 \\
&= \tfrac{1}{4}\sum_{m,m'} \sin\left((m'-m)\varphi\right)\left(A^*_{+m}A_{+m'}\right) i^{(m'-m+1)} \quad .
\end{aligned}
\tag{B.18}
$$

Appendix C

Comparison of analytical results and numerical approach for cylindrical wave case

Here we make a comparison of analytical results and numerical approach for cylindrical wave case. At first, we use the sliced numerical method to solve the incident cylindrical wave problem.

We replace plane wave with cylindrical wave and then the total wave function outside the disk is given by

$$
\begin{aligned}
&\psi_t(r,\varphi) \\
&= \sum_{m,m'} \begin{pmatrix} \int_0^{2\pi} d\delta a(\delta) H_m^{(1)}(\gamma r) e^{im(\delta+\varphi)} \\ \int_0^{2\pi} d\delta a(\delta)(ie^{i\delta}) H_{m'}^{(1)}(\gamma r) e^{im'(\delta+\varphi)} \end{pmatrix} + \sum_{m,m'} \begin{pmatrix} \int_0^{2\pi} d\delta' b(\delta') H_m^{(1)}(\gamma' r) e^{im(\delta'+\varphi)} \\ \int_0^{2\pi} d\delta' b(\delta')(-ie^{i\delta'}) H_{m'}^{(1)}(\gamma' r) e^{im'(\delta'+\varphi)} \end{pmatrix} \\
&+ \begin{pmatrix} \frac{i^{m_{in}}}{2\sqrt{2}} H_{m_{in}}^{(2)}(\gamma r) e^{im_{in}\varphi} \\ \frac{i^{(m_{in}-1)}}{2\sqrt{2}} (R_{in}) H_{m_{in}-1}^{(2)}(\gamma r) e^{i(m_{in}-1)\varphi} \end{pmatrix}
\end{aligned}
\tag{C.1}
$$

where the corresponding ratio R_{in} is -1 and the last term in Eq. (C.1) is the incident

cylindrical wave. For a hard wall boundary condition, the total wave function is zero.

$$\psi_t(R,\varphi) = \sum_{m,m'} \begin{pmatrix} e^{im\varphi}\int_0^{2\pi} d\delta a(\delta) H_m^{(1)}(\tilde{\gamma}) e^{im\delta} \\ e^{im'\varphi}\int_0^{2\pi} d\delta a(\delta)(i) H_{m'}^{(1)}(\tilde{\gamma}) e^{i(m'+1)\delta} \end{pmatrix} + \sum_{m,m'} \begin{pmatrix} e^{im\varphi}\int_0^{2\pi} d\delta' b(\delta') H_m^{(1)}(\tilde{\gamma}') e^{im\delta'} \\ e^{im'\varphi}\int_0^{2\pi} d\delta' b(\delta')(-i) H_{m'}^{(1)}(\tilde{\gamma}') e^{i(m'+1)\delta'} \end{pmatrix} + \begin{pmatrix} e^{im_{in}\varphi}\frac{i^{m_{in}}}{2\sqrt{2}} H_{m_{in}}^{(2)}(\tilde{\gamma}) \\ e^{i(m_{in}-1)\varphi}\frac{i^{m_{in}}}{2\sqrt{2}}(i) H_{m_{in}-1}^{(2)}(\tilde{\gamma}) \end{pmatrix} = 0 \tag{C.2}$$

Here we use the orthogonal relation on the summations of the two component matrix since the "hard" wall boundary is independent.

$$\frac{1}{2\pi}\int_0^{2\pi} d\varphi e^{-im''\varphi}\psi_t = \begin{pmatrix} \int_0^{2\pi} d\delta a(\delta) H_{m''}^{(1)}(\tilde{\gamma}) e^{im''\delta} \\ \int_0^{2\pi} d\delta a(\delta)(i) H_{m''}^{(1)}(\tilde{\gamma}) e^{i(m''+1)\delta} \end{pmatrix} + \begin{pmatrix} \int_0^{2\pi} d\delta' b(\delta') H_{m''}^{(1)}(\tilde{\gamma}') e^{im''\delta'} \\ \int_0^{2\pi} d\delta' b(\delta')(-i) H_{m''}^{(1)}(\tilde{\gamma}') e^{i(m''+1)\delta'} \end{pmatrix} + \begin{pmatrix} \frac{i^{m_{in}}}{2\sqrt{2}} H_{m_{in}}^{(2)}(\tilde{\gamma})\delta_{m_{in}m''} \\ \frac{i^{m_{in}}}{2\sqrt{2}}(i) H_{m_{in}-1}^{(2)}(\tilde{\gamma})\delta_{(m_{in}-1)m''} \end{pmatrix} = 0 \tag{C.3}$$

where $\delta_{mm'} = \frac{1}{2\pi}\int_0^{2\pi} d\varphi e^{i(m'-m)\varphi}$ is delta function. The continuous integration in Eq. (C.3) can be viewed as the discrete summation so that we obtain $\int_0^{2\pi} d\delta \to \sum_{n=1}^{N} \Delta\delta$ where $\Delta\delta = \frac{2\pi}{N} = \Delta\delta'$ and $\delta_n = n\Delta\delta = n\Delta\delta' = \delta'_n$. To simplify formula, we replace $a(\delta_n)$ and $b(\delta_n)$ with a_n and b_n. After simplification, we obtain two equations as following

$$\sum_{n=1}^{N} a_n H_{m''}^{(1)}(\tilde{\gamma}) e^{im''\delta_n} + \sum_{n=1}^{N} b_n H_{m''}^{(1)}(\tilde{\gamma}') e^{im''\delta_n} = -\frac{1}{\Delta\delta}\frac{i^{m_{in}}}{2\sqrt{2}} H_{m_{in}}^{(2)}(\tilde{\gamma})\delta_{m_{in}m''} \tag{C.4a}$$

$$\sum_{n=1}^{N} a_n H_{m''}^{(1)}(\tilde{\gamma}) e^{i(m''+1)\delta_n} - \sum_{n=1}^{N} b_n H_{m''}^{(1)}(\tilde{\gamma}') e^{i(m''+1)\delta_n} = -\frac{1}{\Delta\delta}\frac{i^{m_{in}}}{2\sqrt{2}} H_{m_{in}-1}^{(2)}(\tilde{\gamma})\delta_{(m_{in}-1)m''} \tag{C.4b}$$

From Eq. (C.11), the matrix $FX = G$ can be evaluated

Next, we use the analytical non-slices method to solve the incident cylindrical wave problem. Then the total wave function outside the disk is given by

$$\psi_t(r,\varphi) = \begin{pmatrix} e^{im\varphi} a_m H_m^{(1)}(\gamma r) \\ e^{i(m-1)\varphi} i a_m H_{m-1}^{(1)}(\gamma r) \end{pmatrix} + \begin{pmatrix} e^{im\varphi} b_m H_m^{(1)}(\gamma' r) \\ e^{i(m-1)\varphi}(-i) b_m H_{m-1}^{(1)}(\gamma' r) \end{pmatrix} + \begin{pmatrix} e^{im_{in}\varphi} \frac{i^{m_{in}}}{2\sqrt{2}} H_{m_{in}}^{(2)}(\gamma r) \\ e^{i(m_{in}-1)\varphi} \frac{i^{m_{in}-1}}{2\sqrt{2}} R_{in} H_{m_{in}-1}^{(2)}(\gamma r) \end{pmatrix} \tag{C.5}$$

For a hard wall boundary condition , the total wave function is zero .

$$\psi_t(R,\varphi) = \begin{pmatrix} e^{im_{in}\varphi} a_{m_{in}} H_{m_{in}}^{(1)}(\tilde{\gamma}) \\ e^{i(m_{in}-1)\varphi} i a_{m_{in}} H_{m_{in}-1}^{(1)}(\tilde{\gamma}) \end{pmatrix} + \begin{pmatrix} e^{im_{in}\varphi} b_{m_{in}} H_{m_{in}}^{(1)}(\tilde{\gamma}') \\ e^{i(m_{in}-1)\varphi}(-i) b_{m_{in}} H_{m_{in}-1}^{(1)}(\tilde{\gamma}') \end{pmatrix} + \begin{pmatrix} e^{im_{in}\varphi} \frac{i^{m_{in}}}{2\sqrt{2}} H_{m_{in}}^{(2)}(\tilde{\gamma}) \\ e^{i(m_{in}-1)\varphi} \frac{i^{m_{in}}}{2\sqrt{2}} i H_{m_{in}-1}^{(2)}(\tilde{\gamma}) \end{pmatrix} = 0 \tag{C.6}$$

After calculation, we obtain as following

$$a_{m_{in}} H_{m_{in}}^{(1)}(\tilde{\gamma}) + b_{m_{in}} H_{m_{in}}^{(1)}(\tilde{\gamma}') = -\frac{i^{m_{in}}}{2\sqrt{2}} H_{m_{in}}^{(2)}(\tilde{\gamma}) \delta_{m_{in} m''} \tag{C.7a}$$

$$a_{m_{in}} H_{m_{in}-1}^{(1)}(\tilde{\gamma}) - b_{m_{in}} H_{m_{in}-1}^{(1)}(\tilde{\gamma}') = -\frac{i^{m_{in}}}{2\sqrt{2}} H_{m_{in}-1}^{(2)}(\tilde{\gamma}) \delta_{(m_{in}-1) m''} \tag{C.7b}$$

where $m = m_{in}$ and we define $\tilde{\gamma} \equiv \gamma R$ and $\tilde{\gamma}' \equiv \gamma' R$.

($\delta_{mm''}$ is delta function [30])

The unknown coefficients a_m and b_m can be evaluated by solving Eq. (C.5).

$$a_m = a_{m_{in}} = -\frac{i^m}{2\sqrt{2}} \frac{H_m^{(1)}(\tilde{\gamma}')H_{m-1}^{(2)}(\tilde{\gamma}) + H_m^{(2)}(\tilde{\gamma})H_{m-1}^{(1)}(\tilde{\gamma}')}{H_m^{(1)}(\tilde{\gamma})H_{m-1}^{(1)}(\tilde{\gamma}') + H_m^{(1)}(\tilde{\gamma}')H_{m-1}^{(1)}(\tilde{\gamma})} \tag{C.8a}$$

$$b_m = b_{m_{in}} = \frac{i^m}{2\sqrt{2}} \frac{H_m^{(1)}(\tilde{\gamma})H_{m-1}^{(2)}(\tilde{\gamma}) - H_m^{(2)}(\tilde{\gamma})H_{m-1}^{(1)}(\tilde{\gamma})}{H_m^{(1)}(\tilde{\gamma})H_{m-1}^{(1)}(\tilde{\gamma}') + H_m^{(1)}(\tilde{\gamma}')H_{m-1}^{(1)}(\tilde{\gamma})} \tag{C.8b}$$

We compare Eq. (C.2) with Eq. (C.5) after slicing and then we can obtain a relation of coefficients.

$$\begin{aligned} a(\delta) = a(\delta_n) = a_n = a_m \tfrac{1}{2\pi} e^{-im\delta_n} \\ b(\delta') = b(\delta'_n) = b_n = b_m \tfrac{1}{2\pi} e^{-im\delta'_n} \end{aligned} \tag{C.9}$$

We present here the comparison of analytical results and numerical approach for cylindrical wave case with the wave property m_{in} for different the number of slices N. In following series of figures that the red $*$ line is the numerical approach and the black $\bigcirc$ line is the analytical result. We find that a given larger m_{in} corresponds to a lager N before diverging.

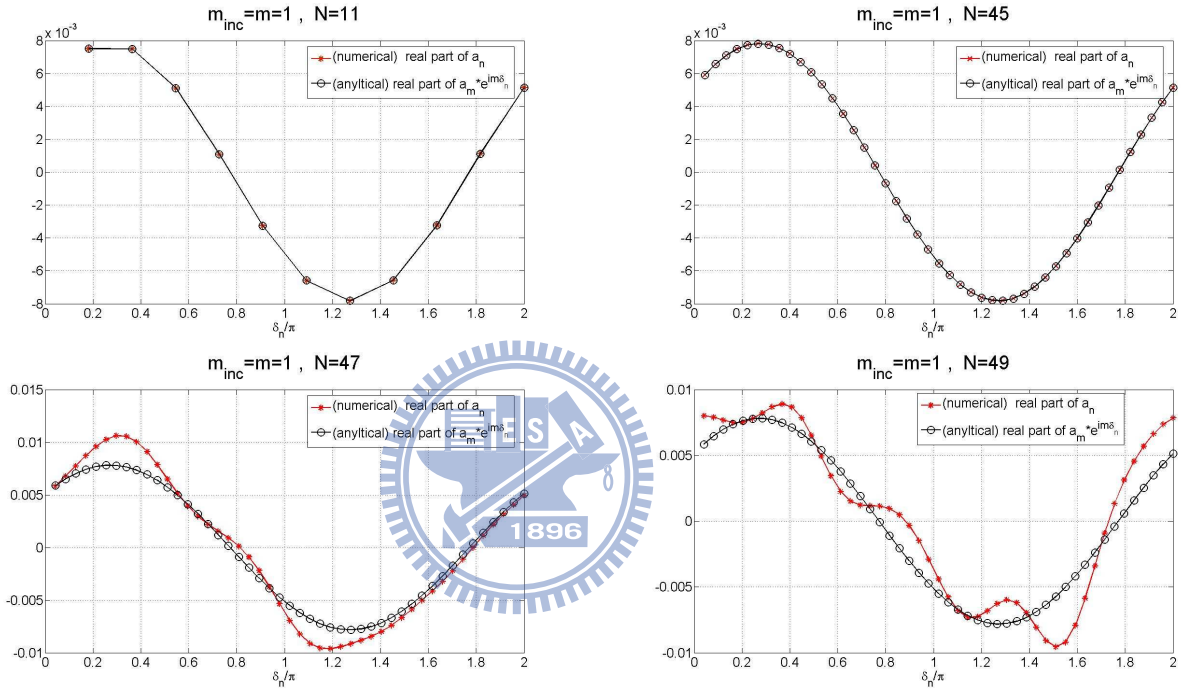

Figure C.1: Comparison of analytical results and numerical approach for cylindrical wave case of m_{in}=1: (a) $N = 11$, (b) $N = 45$, (c) $N = 47$ and (d) $N = 49$.

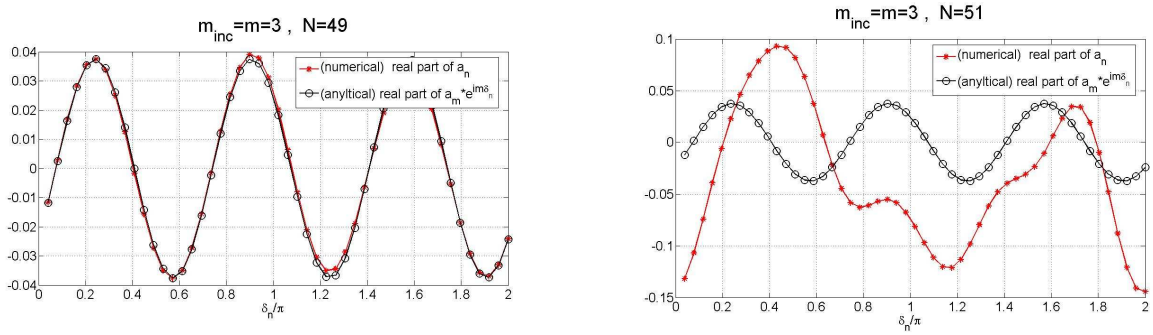

Figure C.2: Comparison of analytical results and numerical approach for cylindrical wave case of m_{in}=3 : (a) $N = 49$ and (b) $N = 51$.

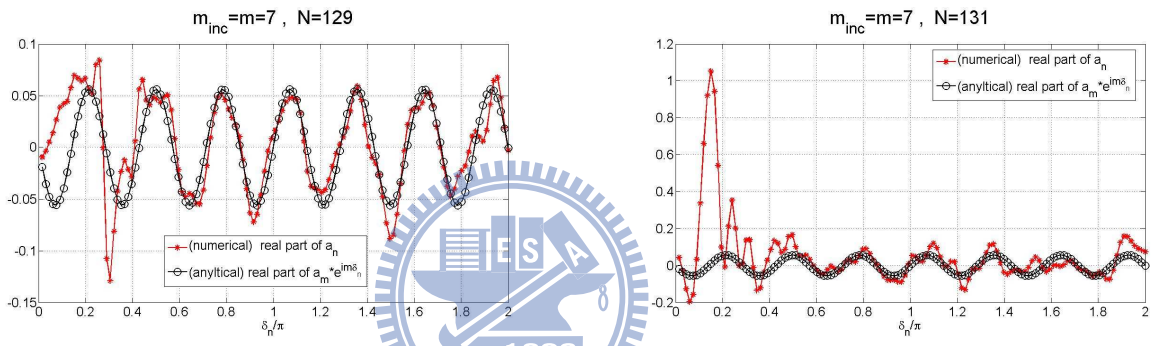

Figure C.3: Comparison of analytical results and numerical approach for cylindrical wave case of m_{in}=7: (a) $N = 129$ and (b) $N = 131$.

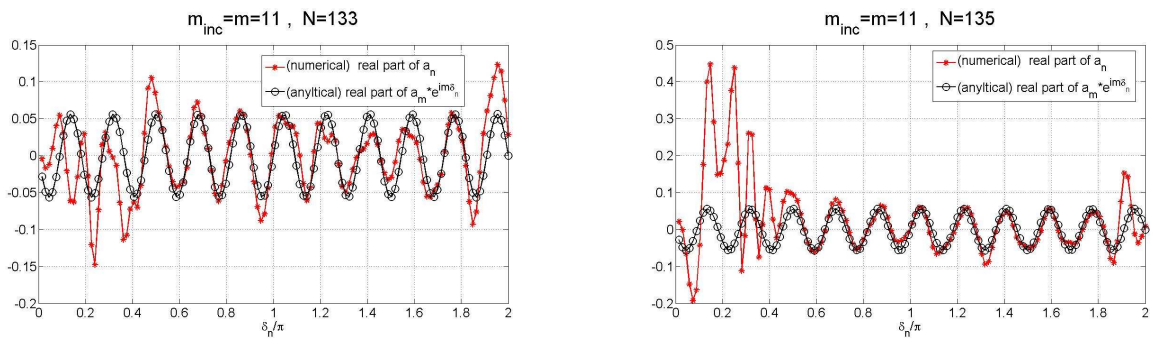

Figure C.4: Comparison of analytical results and numerical approach for cylindrical wave case of m_{in}=11 : (a) $N = 133$ and (b) $N = 135$.

Here the matrix from Eq. (C.11) can be decomposed into small matrix combination.

$$FX = G$$

$$F = \begin{pmatrix} F_{11} & F_{12} \\ F_{21} & F_{22} \end{pmatrix}$$

The unknown coefficients of X can be obtained by solving $X = F^{-1}G$. Also, we assume that

$$F^{-1} = H = \begin{pmatrix} H_{11} & H_{12} \\ H_{21} & H_{22} \end{pmatrix}. \tag{C.10}$$

So the element of F can be in terms of the element of H where

$$H_{11} = \left(F_{11} - F_{12}F_{22}^{-1}F_{21}\right)^{-1} \tag{C.11a}$$

$$H_{22} = \left(F_{22} - F_{21}F_{11}^{-1}F_{12}\right)^{-1} \tag{C.11b}$$

$$H_{12} = -F_{11}^{-1}F_{12}H_{22} \tag{C.11c}$$

$$H_{21} = -F_{22}^{-1}F_{21}H_{11} \tag{C.11d}$$

. To do the matrix simplification, we have a bigger N for a given $m_{in} = 1$.

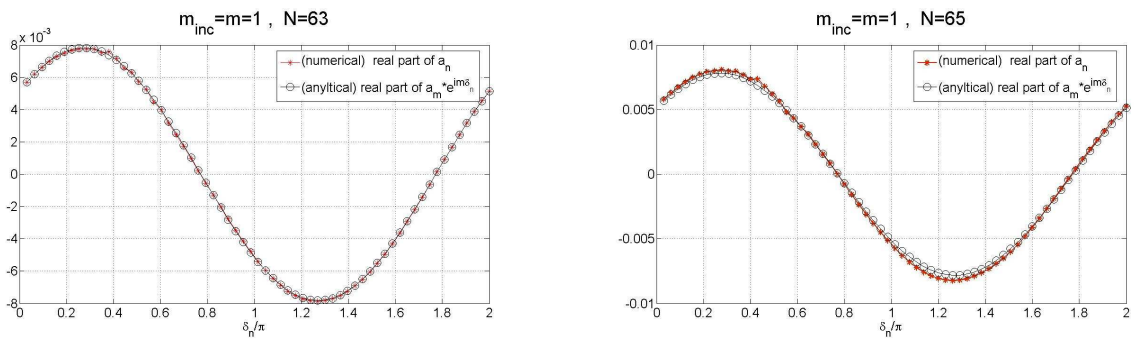

Figure C.5: Comparison of analytical results and numerical approach for cylindrical wave case of m_{in}=1 : (a) $N = 63$ and (b) $N = 65$.

Bibliography

[1] M. I. Dyakonov, V. A. Marushchak, V. I. Perel, and A. N.Titkov, Sov. Phys. JETP. **63** 655 (1986).

[2] *Spin-Orbit Coupling in Two-Dimensional Electron and Hole systems*, Roland Winkler (Springer, 2003).

[3] E. I. Rashba, Fiz. Tverd. Tela (Leningrad) **2**, 1224 (1960) [Sov. Phys. Solid State **2**, 1109 (1960)]; Y. A. Bychkov and E. I. Rashba, J. Phys. C **17**, 6039 (1984).

[4] G. Dresselhaus, Phys. Rev. **100**, 580 (1955).

[5] B. A. Bernevig, J. Orenstein, and S.-C. Zhang, Phys. Rev. Lett. **97**, 236601 (2006).

[6] M. Ohno and K. Yoh, Phys. Rev. B **77**, 045323 (2008).

[7] R. G. Nazmitdinov, K. N. Pichugin, and M. Valn-Rodrguez, Phys. Rev. B **79**, 193303 (2009).

[8] K. Y. Chen, C. S. Chu, and A. G. Malshukov , Phys. Rev. B **71**, 121308 (2005).

[9] John Schliemann and Daniel Loss , Phys. Rev. B **76**, 165311 (2003).

[10] A. O. Govorov, A. V. Kalameitsev, and J. P. Dulka, Phys. Rev. B **70**, 245310 (2004).

[11] J. Cserti, A. Csords, and U. Zlicke, Phys. Rev. B **70**, 233307 (2004).

[12] S. Datta and B. Das, Appl. Phys. Lett. **56**, 665 (1990).

[13] R. G. Nazmitdinov, K. N. Pichugin, and M. Valn-Rodrguez, Phys. Rev. B **79**, 193303 (2009).

[14] J. S. Sheng and Kai Chang Phys. Rev. B **74**, 235315 (2006).

[15] Miao Wang and Kai Chang Phys. Rev. B **77**, 125330 (2008).

[16] Ming-Che Chang , Phys. Rev. B **71**, 085315 (2005).

[17] J. Schliemann, J. C. Egues, and D. Loss, Phys. Rev. Lett. **90**, 146801 (2003).

[18] Jamie D. Walls, Jian Huang, Robert M. Westervelt,2,3 and Eric J. Heller, Phys. Rev. B **71**, 035325 (2006).

[19] J. E. Hirsch, Phys. Rev. Lett. **83**, 1834 (1999).

[20] J. Wunderlich *et al.*, Phys. Rev. Lett. **94**, 047204 (2005).

[21] J. J. Krich and B. I. Halperin, Phys. Rev. Lett. **98**, 226802 (2007).

[22] Y. Li, and R.Tao, Phys. Rev. B **75**, 075319 (2007).

[23] Qing-feng Sun, and X. C. Xie, Phys. Rev. B **72**, 245305 (2005).

[24] Junren Shi, Ping Zhang, Di Xiao, and Qian Niu, Phys. Rev. Lett. **96**, 076604 (2006).

[25] S. K. Adhikari, Am. J. Phys. **54**, 362 (1986).

[26] A. Pályi, C. Péterfalvi, and J. Cserti, Phys. Rev. B **74**, 73305 (2006).

[27] A. Pályi, C. Péterfalvi, and J. Cserti, Phys. Rev. B **76**, 035331 (2007).

[28] J. Y. Yeh, M. C. Chang, and C. Y. Mou, Phys. Rev. B **73**, 35313 (2006).

[29] *Modern Quantum Mechanics, Revised ed.*, J. J. Sakurai (Addison-Wesley, 1994).

[30] *Mathematical Methods for Physicists, 4th ed.*, G. B. Arfkan and H. J. Weber (Academic Press, 1995).